Study on Bimolecular Chemical Reactions under the Bulk and Reactant-Pair Conditions

KAZUHIRO HONDA

The Graduate University for Advanced Studies
(Institute for Molecular Science)
Myodaiji, Okazaki 444, Japan

Contents

1. Introduction 1

2. Experimental 11

A. Instrumental 11

A-1. Bulk experiments 11

A-2. Molecular beam experiments 13

B. Production of hot hydrogen (H) and ground-state oxygen ($O(^3P_J)$) atoms 15

C. Analysis 17

3. Results and discussion 20

A. The H + H_2O reaction under the bulk and reactant-pair conditions 20

A-1. Energetic 20

A-2. Examination of collisional conditions in the bulk experiments 20

A-3. LIF spectra 21

A-4. Relaxation in the $A^2\Sigma^+$ state of OH 22

A-5. Rotational distribution of OH and OD 24

A-6. Reaction mechanism 25

A-7. Energy partition 27

A-8. Population over the spin-orbit components 29

A-9. Population over the Λ-doublet levels 30

A-10. Surprisal analysis 32

A-11. H+H_2O reaction under the reactant-pair condition 35

B. The $O(^3P_J)$ + H_2S reaction under the bulk condition 38

B-1. Energetic 38

B-2. Examination of experimental condition for the bulk experiments 38

B-3. LIF spectra and rotational distribution of OH 39

B-4. Reaction mechanism 40

B-5. Population over the spin-orbit components 41

B-6. Population over the Λ-doublet levels 43

B-7. Suprisal analysis 44

C. The H + N_2O reaction under the reactant-pair condition 46

4. Conclusions 53

A. The $H+H_2O$ reaction under the bulk and reactant-pair conditions 53

B. The $O(^3P)+H_2S$ reaction under the bulk condition 54

C. The $H+N_2O$ reaction under the reactant-pair condition 55

5. Acknowledgment 57

6. Reference 58

1. Introduction

Experimental approaches for studying the dynamics of elementary chemical reactions in microscopic detail have expanded the range of their application dramatically in recent years as a result of the development of various laser sources. The use of lasers for studying the dynamics of chemical reaction has several advantages; the technique of laser photolysis for production of hot atoms provides a narrow distribution of translational energy of reactants. The translational energy can be varied selectively by changing the wavelength of a photolysis laser. Application of laser spectroscopic methods, such as laser-induced fluorescence (LIF), multiphoton ionization (MPI), coherent anti-Stokes Raman scattering (CARS), infrared absorption and emission measurements, makes it possible to measure the internal state distribution of reaction products.

Energy released in the chemical reactions is partitioned into various degrees of freedom of the products. The mode of partition is determined by dynamical interactions operating during the course of chemical reaction. Therefore, for the purpose of elucidation of the dynamics of chemical reaction, it is important to examine the internal state distribution of the reaction products under well-defined reaction energy.

In this thesis, the internal state distribution of OH produced in some elementary chemical reactions was studied using

the LIF technique. The LIF technique using single photon process is more straightforward than the other spectroscopic methods using multiphoton processes, because the former enables one to determine the distribution directly through the Einstein B coefficient. The time resolution of detection is of the order of 10 ns, which is high enough to measure the nascent internal state distribution of reaction products under the molecular beam and flow-cell condition. The spectral resolution is also sufficient to resolve the rotational transitions of OH allowing us the detailed determination of the vibrational and rotational distributions.

We employed the laser photolysis method to produce a high-energy reactant with well-defined energy of reaction. This allows us the precise determination of the available energy or excess energy which can be used to excite the internal states of the products.

Importance of the orientational effect of reactants in the reaction dynamics is well recognized and has been studied under the crossed molecular beam conditions with the application of external electric fields to align the reactant molecule [1]. Recently, studies of the orientational effect with information of the internal state distribution was achieved by a new technique, which used binary van der Waals-type complexes as precursors [2]. We shall hereafter call this type of reaction as the "reactant-pair" reaction. This technique is capable of controlling the

impact parameter and angular orientation in the corresponding bimolecular reaction by restricting the relative orientation of reactant molecules by complex formation. On the basis of structural and dynamical information of the weakly-bound complexes being accumulated recently [3], we expect to obtain a specific information on the reaction dynamics of this type of reactions. A comparison between the bimolecular and reactant-pair reactions will give us useful information on the details of reaction dynamics. The results can also be compared with the results with ab initio methods and dynamical simulations using quantum and quasiclassical techniques.

In this thesis, three elementary reactions

$$H + H_2O \rightarrow OH + H_2$$

$$O + H_2S \rightarrow OH + HS$$

and

$$H + N_2O \rightarrow OH + N_2$$

are studied under the bulk and reactant-pair conditions. The endothermic reaction,

$$H + H_2O \rightarrow OH + H_2 \qquad \Delta H=62.8 \text{ kJ/mol} \qquad (1)$$

is interesting since it is the reverse reaction of $OH + H_2 \rightarrow H_2O + H$, which is an important chain branching step in the hydrogen combustion [4]. Kleinermanns and Wolfrum reported the rotational distribution of OH produced in reaction (1) [5]. They produced

the hot hydrogen atom by photodissociating HBr at 193 nm and probed the rotational state distribution of OH with the LIF technique. On the other hand, we have studied reaction (1) by producing hot hydrogen atoms with the photodissociation of HI at 266 nm. A comparison of different excess energies would provide more detailed information on the reaction mechanism of (1) around the transition state.

The 266 nm photodissociation has an additional advantage. It yields the iodine atom in two spin-orbit states ($^2P_{3/2}$ and $^2P_{1/2}$), corresponding to the translational energies of the hot hydrogen atom of 160 and 70 kJ/mol, respectively [6], instead of 250 and 200 kJ/mol, respectively, for the photodissociation of HBr at 193 nm [6]. Since the translational energy of 70 kJ/mol is less than the estimated reaction barrier of 90 kJ/mol for this reaction [7], the contribution of this channel to the OH production is expected to be minor, most of the OH being produced through the I($^2P_{3/2}$) channel. This situation would simplify the analysis considerably.

In addition, it is interesting to confirm experimentally whether reaction (1) proceeds through a direct mechanism or an indirect mechanism. Here, the direct and indirect mechanism are defined as follows. In the direct mechanism, a hot hydrogen strips off one of the hydrogens in a water molecule instantaneously upon collision. On the other hand, the indirect mechanism is characterized by the existence of a long-lived

intermediate, H_3O. To examine which mechanism is relevant for (1), the reaction of H with D_2O has also been studied. If reaction (1) occurs indirectly, it would produce both OH and OD radicals, whereas the direct process would produce only the OD radical.

In order to study the orientational effect of bimolecular reaction (1), we performed a supersonic free jet experiment for the following reactant-pair reaction,

$$BrH{\cdot}H_2O + h\nu \rightarrow (H \rightarrow H_2O) + Br \rightarrow OH + H_2 + Br \qquad (2)$$

The information of the geometrical configuration of this complex is important to analyze the reaction dynamics under the reactant-pair conditions. Unfortunately, the structural information of the $HX{\cdot}H_2O$ complex is restricted to $HF{\cdot}H_2O$ and $HCl{\cdot}H_2O$, which have been studied by using microwave spectroscopy [8] . These results suggest that the hydrogen in HX (X=F,Cl) is bonded to the oxygen atom to form a planar complex. Ab initio calculations of $HBr{\cdot}H_2O$ complex [9] suggest that the potential energy surface has two minima ($H_2O{\cdots}HBr$ and $HBr{\cdots}OH_2$). The first minimum, $H_2O{\cdots}HBr$, is more stable by 16.2 kJ/mol than the second, $HBr{\cdots}OH_2$. They are illustrated in Fig. 1.

The $O(^3P_J)$ + H_2S reaction studied under the bulk condition is the second target in this thesis. The exothermic reaction of the ground-state oxygen atom with H_2S proceeds via the hydrogen abstraction and additional-displacement channel;

$$O(^3P_J) + H_2S \rightarrow OH + SH \qquad \Delta H=-43 \text{ kJ/mol} \qquad (3)$$

$$\rightarrow HSO + H \qquad \Delta H=-16 \text{ kJ/mol} \qquad (4)$$

Experimental results under the bulk condition [10] have suggested that OH formation is the main channel (≈52%), while the additional-displacement channel leading to HSO is less than 11%.

Reaction (3) can be classified one of the "heavy-light-heavy" (H-L-H′) mass combination cases. We assume that O attacks one of the H-S bond in H_2S while the other H-S bond is unaffected (the "spectator-stripping" mechanism). The "H-L-H′" system has been studied experimentally [11] and theoretically [12]. These results suggest that the energy partition among the internal states of products is kinematically constrained; for example, the little product rotational excitation and the strong vibrational excitation which would sometimes result in a population inversion in the case of exothermic reactions. This point will be discussed in section 3.B.

The relative population of the spin-orbit states of the oxygen atom was recently measured for the photodissociation of NO_2 at 355 nm by using a two-photon LIF technique under the bulk condition [13]. The population ratio $^3P_2$:$^3P_1$:$^3P_0$ of $O(^3P_J)$ is 1.0:0.18:0.04. This result suggests that the distribution of $O(^3P_J)$ (J=2,1 and 0) by the 355 nm photodissociation is of Boltzmann. We shall discuss later, on the basis of our experimental result, if this population ratio is retained in the

population of the spin-orbit states in the product OH radical. This would give us a unique opportunity to discuss the possibility of angular momentum conservation in this type of reaction.

It is interesting to compare the Λ-doublet formation of the OH radical in the $O+H_2S$ system with that in the $H+H_2O$ system. If the direct hydrogen abstraction is assumed, the $H+H_2O$ system gives OH which has its origin in the "old" bond of the water molecules. The π orbital of the dissociating OH fragment may then retain some memory before collision. Therefore, we could expect some preferential population in the Λ-doublet components of OH. On the other hand, in the $O+H_2S$ reaction, the OH radical is newly formed as the result of reaction. The resulting OH may not display any Λ-doublet selectivity due to the reactant molecular structure. It would, however, exhibit some dynamical preference due to the mode of collision between O and H_2S.

The third topic studied in this thesis is the $H+N_2O$ reaction under the reactant-pair condition. The bimolecular reaction of the hydrogen atom with N_2O may proceed through the following channels [14]:

$$H + N_2O \rightarrow OH(X^2\Pi) + N_2(X^1\Sigma) \quad (5)$$

$$\Delta H = -262.9 \text{ kJ/mol}$$

$$\rightarrow OH(A^2\Sigma) + N_2(X^1\Sigma) \quad (6)$$

$$\Delta H = 128.1 \text{ kJ/mol}$$

$$\rightarrow NH(X^3\Sigma) + NO(X^2\Pi) \quad (7)$$

ΔH=134.0 kJ/mol

where channel (5) is highly exothermic, while channels (6) and (7) are endothermic.

An ab initio calculation [14] has suggested the existence of the "direct" and "indirect" pathways for channel (5) as shown in Fig. 2. The direct pathway is the attack of a hydrogen atom to the oxygen end of N_2O. The calculated barrier is 79 kJ/mol [14]. On the other hand, the indirect path is the attack of a hydrogen atom to the nitrogen end of N_2O to form a long-lived NNOH intermediate at a shallow potential well (131 kJ/mol) [14]. The calculation for the indirect process has suggested the existence of two barriers on the entrance and exit channels with barrier heights of 11 kJ/mol and 65 kJ/mol [14], respectively.

In this thesis, the following photochemical reaction will be examined;

$$HI{\cdot}N_2O + h\nu(248\ nm) \rightarrow OH(X^2\Pi) + N_2(X^1\Sigma) + I \qquad (8)$$

with the $HI{\cdot}N_2O$ complex produced in a pulsed supersonic jet. We measured the rotational distribution of $OH(X^2\Pi)$ produced in channel (8) by using the LIF technique.

The structure of $HI{\cdot}N_2O$ has not been determined experimentally. If we assume two (or three) comformers by the analogy of $HX{\cdot}N_2O$ (X=F, Cl and Br) [15] as shown in Fig. 3, we

can monitor two channels, corresponding to the formation of I and I^* , for each conformer. For the type (1) and (2) conformations (Fig. 3), we would expect the "direct" channel corresponding to the bimolecular reaction. In this case, the hydrogen atom attacking N_2O with the specific values of the collision parameters would provide a specific distribution of energy over the product internal and translational degrees of freedom. On the other hand, for the type (3) conformation (Fig. 3), we would expect the "indirect" channel. Similar to the bimolecular reaction, the resultant distribution would be governed mostly by a statistical factor, because the intermediate has relatively long lifetime for the energy randomization.

Dissociation of HI at 248 nm yields the I atom in two spin-orbit states ($^2P_{3/2}$ and $^2P_{1/2}$, in the ratio 0.75 : 1 [6]), corresponding to the relative translational energies of the hydrogen atom of 183 and 96 kJ/mol, respectively. Both channels have the translational energies greater than the predicted barriers to the attack of hydrogen to the terminal N and O of N_2O. This situation would make the analysis difficult, because the obtained LIF spectrum is a superposition from plural channels.

Hollingsworth et al. have reported the rotational distributions of $OH(X^2\Pi)$ by the photolysis of HI at 248 nm under the bulk condition [16]. Their experimental results suggest that the rotational distribution of OH is a superposition of two

Boltzmann distributions characterized by the rotational temperatures of 1100 ± 100 and 4700 ± 300 K.

Ohoyama et al. have studied the photochemical reaction of $HI \cdot N_2O$ under the reactant-pair and bimolecular conditions by the 266 nm laser irradiation [17]. The rotational distribution obtained for the reactant-pair reaction is a superposition of three Boltzmann distributions, while it is characterized by two Boltzmann distributions in the case of the bimolecular reaction. They have suggested the channel producing I^* gives rise to insufficient energy to overcome the barrier and that the plural Boltzmann distributions are explained in terms of the existence of two geometrically isomeric complexes (type (2) and (3) in Fig. 3).

2. Experimental

A. Instrumental

The experimental method employed here involves generation of high kinetic energy ("hot") atoms by laser photolysis of the precursor molecules (HI, HBr and NO_2). These hot atoms give a sufficient energy to overcome the reaction barrier so that the reaction can proceed at the room temperature. The internal state distribution of the product OH radical is detected by the LIF measurement.

A-1. Bulk experiments

Fig. 4 shows a schematic diagram of the experimental setup for the experiment under the bulk reaction. The measurement was carried out at the room temperature (294-296 K). The gaseous sample was continuously flowed into a stainless-steel reaction chamber and irradiated by pulsed lasers operated at 10 Hz. The repetition rate of laser pulses was such that the whole irradiated gas was pumped out completely before the next laser pulse. The gaseous reactants were mixed just before the reaction chamber in a 1:1 ratio. The total gas pressure was varied from 10 to 100 mTorr as monitored by a capacitance manometer (MKS Baratron 220B, 0-1 Torr).

The fourth harmonic output (266 nm) of a Nd:YAG laser

(Quantel 51-C) was used to photolyze hydrogen halides. The third harmonic output (355 nm) of a Nd:YAG laser (Quanta-Ray DCR2A) was used to photolyze NO_2. The LIF probe pulse was supplied by the doubled output of a dye laser (Lambda Physik FL3002; band width 0.2 cm^{-1}) pumped by a XeCl excimer laser (Lumonics HE-420-SM-B). The dye laser was operated with kiton red and sulforhodamin 640 in the 306-323 nm region to excite the OH $A^2\Sigma$-$X^2\Pi$ (0-0) and (1-1) transitions of OH. In order to avoid a saturation, the pump- and probe-laser pulse energies were kept at about 3-4 mJ per pulse and 200 μJ per pulse, respectively. The pump- and probe-laser beams were incident from the same direction so that they crossed each other at a small angle.

Fluorescence was detected in the perpendicular direction by a photomultiplier (Hamamatsu R453) through an optical filter (Hoya UV30). The photomultiplier signal was amplified and integrated by a boxcar averaging system (Stanford Research SR240, SR250 and SR235) with the gate width of 0.5-1 μs. The LIF signals were averaged for 100 shots at each wavelength and was scanned at a scan step of 0.00125 nm. In order to avoid scattered light entering into the photomultiplier, the light baffle was used and the gate pulse was delayed by 80-200 ns from the probe pulse. The delay time was also 80-200 ns between the pump- and probe-laser pulses. The relative LIF intensities of the rotational lines were not affected by varying the total pressure between 20 and 100 mTorr, ensuring that the nascent

rotational distribution was obtained. The pump- and probe-laser pulse energies were monitored by photodiodes and used to correct the LIF intensity for energy variation.

HI(Matheson 98%), NO_2(Matheson 99.5%) and H_2S(Seitetsu Kagaku 99.8%) were used without further purification. D_2O (Merck 99.75%) and distilled water were further degassed by the freeze-pump-thaw method.

A-2. Molecular beam experiments

Fig. 5 shows a schematic diagram of the experimental setup for experiments under the reactant-pair conditions. A conventional pulsed valve of 0.8 mm diameter was operated at 10 Hz. The opening time of valve was 1 msec. The $HI{\cdot}N_2O$ complex was generated by expanding a pre-mixed gas, containing 2.6% HI and 4.4% N_2O in 93% He, through a pulsed nozzle into a vacuum chamber. For the $HBr{\cdot}H_2O$ complex production, it was necessary to mix the gaseous samples just before the nozzle to avoid undesired reactions in the nozzle. HBr (2.6%) in He was pre-mixed in a gas reservoir and mixed with 0.9% H_2O in He, prepared by bubbling He in water, just before the nozzle.

The cluster size distribution and time profile were measured 50 cm downstream using a quadrupole mass spectrometer (Extranuclear), which was mounted in a separate chamber differentially pumped by a liquid-nitrogen-trapped diffusion pump. Ionization was made at a low electron energy of 30 eV so

as to suppress fragmentation of clusters. The background pressure in the reaction chamber was kept at 10^{-4} Torr, while the mass chamber was maintained at 10^{-6} Torr. The mass spectroscopic measurements showed that typical duration of the gas pulse is 500 μsec for the monomer species, while cluster species appeared after a significant delay from the rise of the monomer signal with a duration of about 100 μs. The delay did not depend significantly on the cluster size, indicating that it is not due to the difference in velocity but to the delayed formation of the cluster species during the expansion.

The reactant pair $IH \cdot N_2O$ was photolyzed by a KrF eximer laser (LUMONICS EX-510, 248 nm). The reactant pair $BrH \cdot H_2O$ was photolyzed by an ArF excimer laser (LUMONICS EX-510, 193nm). Probe light was provided by a frequency-doubled tunable dye laser (Lambda Physik FL 3002; band width 0.2 cm^{-1}) pumped by a XeCl excimer laser (Lumonics HE-420-SM-B). The dye laser was operated with Kiton red in metanol and its doubled output covered the range of 306-311 nm. It was applied after a short delay (typically 150 ns) from the 248 and 193 nm irradiations, respectively. The pump and probe pulse beams were collinear and intersected the jet 30 mm downstream from the nozzle. Fluorescence from OH was collected by an optical system made of concave mirror and lenses, and focused onto a photomultiplier (Hamamatsu R943-02) through filters (HOYA UV29, UV30 and U340). The OH fluorescence signal arriving 200-900 ns after the probe

pulse was counted by the gated photon counter. HBr(Matheson 98%) and N_2O (Nippon Sanso 99.8%) was used without further purification.

B. Production of hot hydrogen atoms and ground-state oxygen atoms

Absorption bands of HBr between 250 and 160 nm and of HI between 280 and 180 nm are continuous [18] because of repulsive upper states. Photodissociation of HI at 266 nm yields in two spin-orbit states by,

$$HI \rightarrow H + I(^2P_{3/2}) \quad (9)$$

$$\rightarrow H + I^*(^2P_{1/2}) \quad (10)$$

The ratio of the ground-state $I(^2P_{3/2})$ and the first excited-state $I^*(^2P_{1/2})$ channels is 1.8:1 [6]. The energy difference, E_{el}, between the $I(^2P_{3/2})$ and $I^*(^2P_{1/2})$ states is 91 kJ/mol [6].

The total translational energy, $E_{H,I}$, released upon the photodissociation of HI may be expressed as

$$E_{H,I}=E(h\nu)-D_0(H-I)+E_{therm}(HI)-Eel(I) \quad (11)$$

$$\approx 163 \text{ kJ/mol } [I(^2P_{3/2}) \text{ channel}]$$

$$\approx 72 \text{ kJ/mol } [I^*(^2P_{1/2}) \text{ channel}]$$

where $E(h\nu)=449$ kJ/mol is the photon energy of 266 nm radiation, $D_0(H-I)=295$ kJ/mol is the dissociation energy of HI into H and $I(^2P_{3/2})$ [18] and $E_{therm}(HI)$ is the thermal (translational and

internal) energy of HI,

$E_{therm}(HI)=(3/2)RT(translation)+(2/2)RT(rotation)+RT(vibration)$
$=9$ kJ/mol.

By the conservation of linear momentum constraints, the translational energy of H atom, E_H, may be expressed as

$$E_H=(1/2)M_H V_H^2=M_I E_{H,I}/(M_H+M_I) \qquad (12)$$
$$\approx 162 \text{ kJ/mol } [I(^2P_{3/2}) \text{ channel}]$$
$$\approx 71 \text{ kJ/mol } [I^*(^2P_{1/2}) \text{ channel}]$$

where M_i and V_H (i=H and I) are mass and velocity (laboratory frame) of photofragments, respectively. In the center-of-mass frame, the collision energy, E_{coll}, for the $H+H_2O$ collision may be approximated by,

$$E_{coll}=(1/2)\mu(V_H^2 + RT/M_{H2O}) \qquad (13)$$
$$\approx 160 \text{ kJ/mol } [I(^2P_{3/2}) \text{ channel}]$$
$$\approx 69 \text{ kJ/mol } [I^*(^2P_{1/2}) \text{ channel}]$$

where μ is the reduced mass of the $H + H_2O$ system and the second term in the parenthesis represents the average contribution from thermal motion of H_2O. The collision energy of the $H+D_2O$ reaction is almost the same. Similarly, dissociation of HI at 248 nm and of HBr at 193 nm yield the translational energy of H of 185 and 98 kJ/mol in the ratio of 0.75:1, respectively, for the $X(^2P_{3/2})$ channel, and 253 and 205 kJ/mol in the ratio of 5.7 : 1, respectively, for the $X^*(^2P_{1/2})$ channel [6].

The absorption bands of NO_2 in the ultraviolet and visible region are extremely complex and no rotational and vibrational structure is observed under low resolution [18]. In the photolysis of NO_2, a monoenergetic distribution of the oxygen atom translational energy is therefore not expected.

C. Analysis

Assignment of the observed LIF spectra was carried out on the basis of the table of Dieke and Crosswhite [19]. Spin-orbit and orbital-rotation interactions in the $^2\Pi$ state of OH cause fine structure splittings for each rotational level [20] as shown in Fig. 7. Each of these fine structure levels can be probed by monitoring the corresponding subbands, i.e., F_1A' by P_{11}- or R_{11}-, F_1A'' by Q_{11}-, F_2A' by P_{22}- or R_{22}- and F_2A'' by Q_{22}- branches, so that populations in the sublevels can be determined separately. Here F_1 and F_2 denote the spin-orbit component of $OH(^2\Pi)$ corresponding to J=3/2 and 1/2, respectively. A' and A'' represent the Λ-doublet components, where the unpaired electron lies in and perpendicular to the plane of the molecular rotation, respectively [21], as shown in Fig. 6.

The energy level diagram for the $^2\Sigma^+$-$^2\Pi$ transition is shown in Fig. 7, where the analysis by Dieke and Crosswhite [19] is followed. They used the notations for Hund's case (b). The case (b) assumes that the spin couples to the rotation rather than to the internuclear axis [20]. The total angular momentum, J_{OH}, is

expressed as K+1/2 and K-1/2 for the $^2\Pi_{3/2}$ and $^2\Pi_{1/2}$ states, respectively, where K is the total angular momentum quantum number without spin. The selection rules for this transition are $\Delta J=0, \pm1$ and $+\leftrightarrow-$, where the signs represent the total parity of wavefunction. In Hund's case (b), there is an additional selection rule of $\Delta K=0, \pm1$, where $\Delta K=K'-K''$. Lines satisfying both selection rules constitute main branches. Transitions which violate the ΔK rule are the satellite branches. For higher K, where case (b) is a good approximation, the satellite band intensities are negligible compared to the main line intensity, but at lower values of K the intensities are comparable. R-, Q- and P-branches depend on whether ΔK changes by 1, 0, -1, respectively. Therefore, the main branches have $\Delta J=\Delta K$ and this is not true for the satellite lines. The LIF intensity was obtained from the area below each band. For branches with satellites (such as Q_{11} and R_{11}-branches), where main and satellite bands were observed separately for higher K but completely overlapped with each other for lower K, the sum of the main and satellite band areas was determined and divided into the component on the basis of the theoretical Einstein B coefficients [22].

The LIF intensity may be expressed as

$$I_{LIF} \propto I_{Laser} \times B \times P_{vJ}(T) \qquad (14)$$

where I_{Laser} denotes a probe laser power and B represents the

Einstein B coefficient, and P_{vJ} denote the population for each rovibrational state of OH. The relative rotational population can be obtained from the observed I_{LIF} and the tabulated transition probability.

The relative rotational population of OH at temperature T may be expressed as,

$$P_{vJ} \approx (2J+1)\exp(-E_{rot}/RT) \qquad (15)$$

where E_{rot} is the rotational energy for each level, and (2J+1) represents the degeneracy. Equation (15) can be rewritten as

$$1/T = -(R/E_{rot})\ln(P_{vJ}/(2J+1)) \qquad (15)'$$

If the rotational distribution is of Boltzmann type, a linear relation is expected between $\ln(P_{vJ}/(2J+1))$ and E_{rot} and the rotational temperature can be determined from the slope.

3. Results and Discussion

A. The H + H_2O reaction under the bulk and reactant-pair conditions

A-1. Energetic

For the ground-state H+H_2O reaction system, the quasiclassical trajectory calculations have been performed previously [7]. The potential curve along the reaction coordinate is shown in Fig. 8. It is characterized by a large barrier of 90 kJ/mol and a endoergicity of 62 kJ/mol [7]. The levels in the left part of the figure indicate the translational energy of reactants from the photolysis channel of HX (X=Br and I) in the center-of-mass system. To the right shown are possible vibrational states of products with energies less than 160 kJ/mol [7].

A-2. Examination of collisional conditions in the bulk experiments

Fig. 9 shows a plot of the OH LIF signal intensity for the $R_{11}(5)$ line of the (0,0) band as a function of total gas pressure. H_2O and HI are mixed in the 1:1 ratio. The pump-probe and probe-gate delay times are 80 nsec. The linear dependence from 20 to 100 mTorr suggests that there is no effect of rotational relaxation under these pressures.

Fig. 10 shows the ratio of signal intensities,

$R_{11}(5)/R_{11}(6)$, for the (0,0) band vs gas pressure. Here, the experimental conditions are the same as for Fig. 9. This result shows no appreciable change of the ratio as the total pressure increases, suggesting again that there is no effect of collisional relaxation.

Fig. 11 shows the LIF signal intensity of the $R_{11}(5)$ line of the (0,0) band as a function of the pump-probe delay time. Here, the probe-gate delay time is fixed at 80 nsec and the total gas pressure is 60 mTorr (the gas mixture of 30 mTorr H_2O and 30 mTorr HI). This result shows that the signal initially increases linearly with delay until about 500 nsec. This rise time is associated with a flight time of H until it collides with H_2O.

A-3. LIF spectra

Fig. 12 shows the LIF signal intensity vs probe laser power under fixed pump power (4 mJ/pulse). The gas pressure is the same as that for Fig. 11. The delay times are the same as those for Fig. 9. The linear response from 100 to 400 μJ/pulse suggests that the saturation of LIF signal by the probe laser does not occur in this energy range.

Fig. 13(a) shows a part of the LIF spectrum of the (0,0) band of OH produced in the $H+H_2O$ reaction under a typical experimental condition (the total gas pressure and pump-probe delay time are 60 mTorr and 80 nsec, respectively). The horizontal axis shows the wavelength of probe laser. From the

results of fig. 9-fig. 12, we expect that this LIF spectrum reveals nascent population distribution over the $OH(X^2\Pi)$ rotational states. Moreover, we tried to detect vibrationally excited OH radicals. The OH radical in the v"=1 state is expected to be populated on the basis of energetic consideration [7], as shown in fig. 8. However, we could not observe any LIF signal due to the (1,1) transition under the S/N ratio of fig. 13(a).

Fig. 13(b) shows the LIF spectrum for the $H+D_2O$ reaction. The observed band can be assigned entirely to OD [23]. The transition probability of the $(A^2\Sigma^+-X^2\Pi)$ transition of OD is almost the same as that for OH [22]. The $H+H_2O$ and $H+D_2O$ reactions proceed through the same potential surface. It is therefore suggested that reaction (1) with D_2O produces OD almost exclusively. A possible mechanism leading to this result will be discussed in A-6.

A-4. Relaxation in the $A^2\Sigma^+$ state of OH

Electronically excited $OH(A^2\Sigma^+)$ is efficiently deactivated by surrounding water molecules [24].

$$OH(A^2\Sigma^+) + H_2O \rightarrow OH(X^2\Pi) + H_2O \qquad (16)$$

Reaction (16) is a nonradiative process and its rate depends markedly upon rotational level in the $A^2\Sigma^+$ state. Recently, experimental data have been reported for several rotational

levels of the $A^2\Sigma^+$ state, as shown in Fig. 14 [24]. The horizontal and vertical axes show the rotational quantum number and quenching rate constant, respectively. This suggests that the relaxation of higher rotational levels proceeds more slowly than the lower one.

Therefore, the observed LIF spectra must be corrected for the quenching. The rate of quenching of $OH(A^2\Sigma^+)$ is

$$-d[OH(A^2\Sigma^+)]/dt=k[OH(A^2\Sigma^+)][H_2O] \quad (17)$$

where k is the quenching rate constant at 295 K and the brackets denote concentrations. $[H_2O]$ can be treated as a constant since $[H_2O]>>[OH(A^2\Sigma^+)]$. Equation (17) may then be integrated to give

$$[OH(A^2\Sigma^+)]=[OH(A^2\Sigma^+)]_0\times\exp(-k[H_2O]t) \quad (18)$$

where $[OH(A^2\Sigma^+)]_0$ is the concentration of $OH(A^2\Sigma^+)$ at t=0.

Table. 1 shows the results calculated by the equation (18) for the bulk conditions with $[H_2O]=30\times10^{-3}$ Torr and $t=1.08\times10^{-6}$ sec. The decay time of 1.08×10^{-6} sec corresponds to the sum of the probe-gate and gate width. This results suggest that the effect of quenching is considerable. For example, in the case of the K=0 state, a half of the initial concentration of $OH(A^2\Sigma^+)$ is quenched under our experimental condition. However, the relative change of the quenching rate with K is rather small, for example, it varies only about 16 % on going from K=0 to K=11. The LIF intensity used below has been corrected for the quenching

effect both for the $H+H_2O$ and for the $H+D_2O$ reaction. Since the dipole moment of D_2O is 1.85D [25], the quenching rate is expected to be almost the same as that for the $H+H_2O$ reaction. No correction has been made for the collisional quenching by HI, since no data are available. The dipole moment of HI of 0.382D [25] would imply a less significant contribution to the measurement of OH rotational distribution.

A-5. Rotational distribution of OH and OD

Fig. 15 shows the rotational state distributions of OH (v"=0) produced in the $H+H_2O$ reaction for the F_1A', F_2A' and $F_1A"$ manifolds. They are obtained from the analysis of the R_{11}-, R_{22}- and Q_{11}-branch transitions, respectively. In the case of the F_1A' state, the rotational distribution is almost the same as that reported by Kleinermanns and Wolfrum for the 193 nm photodissociation [5]. The rotational state distribution of OD in the $H+D_2O$ reaction is given in Fig. 16, showing a similar dependence on the rotational quantum number to the OH case.

Fig. 17 shows a Boltzmann plot of the data for the $H+H_2O$ reaction in Fig. 15. The horizontal axis shows the rotational energy [19] and the vertical axis shows logarithmic plot of populations divided by the total angular momentum degeneracy, (2J+1). The distributions are of Boltzmann type except for very low rotational levels. The rotational temperatures are 700 ± 50 K and 500 ± 30 K for the F_1A' (F_2A') and $F_1A"$ levels,

respectively. These rotational temperatures correspond to the energies of about 8% and 6 %, respectively, of the available energy (70 kJ/mol). If the initial energy of reactant is statistically partitioned into the whole degrees of freedom of the products, the fraction of energy partitioned into rotation is g_r=(2/2)RT/(3/2)RT+((2/2)RT+RT)+((2/2)RT+RT)=18%. Experimental fraction, 8% or 6%, is fairly lower than the statistical value.

A-6. Reaction mechanism

The non-observation of OH in the H+D_2O reaction suggests strongly that reaction (1) proceeds through the direct mechanism, in which the hot hydrogen attacks one of the hydrogens in H_2O and removes it as H_2 to leave OH. If this reaction proceeded through a long-lived complex, OH should have been formed as well as OD. Direct removal of one of the deuterium atoms in D_2O by H may give rise to an exclusive formation of OD. We shall show below that the direct stripping mechanism accounts for several observations reported here.

From both LIF spectra, we performed the rough estimation of ratio of the cross sections. For the H+H_2O and H+D_2O reactions presented here, the pump and probe laser powers and the crossing area of two lasers have carefully been adjusted to the same conditions. Since the transition probability is almost the same [22], the ratio of sum of LIF line intensities would directly give the ratio of the cross sections for two reactions. From the

sum for the R_{11}-branch transition, the ratio of the cross sections is obtained as

$$I_{OH}/I_{OD} \approx 3.3.$$

Recently, Volpp and Wolfrum have found that the reactive cross section for the $H+H_2O$ is about 2.5 times larger than that for the $H+D_2O$ at the center-of-mass translational energy of 250 and 200 kJ/mol [26], which is in reasonable agreement with our estimation.

Despite the energy accessible for the vibrationally excited OH(v"=1) as shown in Fig. 8, vibrationally excited OH could not be observed. Therefore, as far as the vibrational motion is concerned, this reaction seems to be explained on the basis of the spectator-stripping model; namely, the nonreactive OH" bond is a spectator during the reaction.

Existence of a later barrier has been suggested for the $H+H_2O$ system theoretically [7] and experimentally [27]. The reaction rate should therefore be enhanced by the vibrational excitation of water molecule rather than the excitation of its translational energy. The colliding H atom would form an HH' bond after the H'-O bond distance is elongated.

Fig. 18 shows the transition state geometry of H-H'-O-H" determined by the ab initio calculation [28]. This indicates the nearly collinear approach of colliding H to one of the H-O bond of H_2O. It also suggests that the bond distance between O and H"

is almost the same value as that of the isolated H'OH" (0.9568 Å [29]) and the bond distance between O and H' is elongated. Also, the H'-OH" bond angle on the saddle point is 116.3°, which is similar to that of the isolated H'OH", i.e. 104° [29]. This could support the above-mentioned model of spectator stripping. It also suggests that the rotational excitation of product OH would not be appreciable. Even if there is some torque operating through the OH' bond, the center-of-mass locating close to oxygen would hinder an effective rotational excitation.

A-7. Energy partition

Kleinermanns and Wolfrum have reported the rotational distribution of OH produced in the $H+H_2O$ reaction, where the hot hydrogen atom is produced in the 193 nm photolysis of HBr [5]. HBr decomposed at 193 nm yields two different center-of-mass H atom energies, 260 and 200 kJ/mol corresponding to Br and Br^*, respectively. Although both energies are greater than the $H+H_2O$ barrier, their result for the F_1A' level can be represented by a single Boltzmann with the rotational temperature of 650 K, which corresponds to 3% of the available energy [5]. This may be compared with our results for the H atom produced in the 266 nm photolysis of HI; namely, T_R=700 K and 500 K for F_1A' and $F_1A"$ corresponding to 8% and 6%, respectively, of the available energy. It is interesting to note that the rotational energy partitioned into the F_1A' manifold is almost the same for both

experiments, while the difference of the partition ratio (3% and 8%) arises from the difference of the translational energy of the hot hydrogen (available energy). It is therefore concluded that the rotational excitation in this reaction is insensitive to the translational energy of hot hydrogens. On the other hand, a similar system, $H+O_2 \rightarrow OH+H$, exhibits a dependence on the translational energy of the hot hydrogen [30]. Kesseler and Kleinermanns have also examined the effect of variation of the translational energy using a tunable laser source, obtaining the same conclusion [31].

In order to account for this result, a model of rotational excitation through the bending vibration of H_2O has been proposed [7]. At the time of collision, the H-H'OH" supermolecule on the saddle point may be excited in its bending motion (H'OH"). If we adapt the bending frequency (ω_b) of 1687 cm^{-1} , which is the frequency for the ground-state H_2O [32], the excess energy on saddle point is sufficient to excite the v"=1 state.

We suppose that the torque due to the v"=1 bending vibration can impart a rotational motion to the departing OH" fragment. Because the O atom is 16 times heavier than H, the instantaneous angular momentum of OH" due to the H'OH" bending motion is

$$J_{OH"}=M_{H"}r_{OH"}{}^2\dot{\Theta} \qquad (19)$$

where $M_{H"}$ is the H" atom mass, $r_{OH"}$ is the OH" distance in H'OH" and Θ and $\dot{\Theta}$ are the H'OH" bending angle and its time deviation.

A classical harmonic oscillator model gives

$$\theta=-(h\omega_b/I_b)^{1/2}\ \mathrm{SIN}(\omega_b t) \qquad (20)$$

where I_b is the moment of inertia (roughly $M_{H"}r_{OH"}^2$), ω_b is the bending frequency, and t is the time. The time average of the square of (20) gives

$$\langle\theta\rangle^2=(h\omega_b/I_b)/2 \qquad (20)'$$

The average energy given to the OH rotation is therefore estimated as

$$\begin{aligned}\langle E_{OH}\rangle &= B_e\langle J_{OH}\rangle^2 \\ &= (1/4)h\omega_b \\ &\approx 510\ \mathrm{kJ/mol}\end{aligned} \qquad (21)$$

which corresponds to $T_R\approx$ 600 K. This is in good agreement with the experimental rotational temperatures. If we assume that only the v"=1 bending motion can be excited by collision, the insensitivity of T_R on the excess energy can reasonably explained.

A-8. Population over the spin-orbit components

Fig. 19 shows the ratio of populations in two spin-orbit components, F_1,A′ and F_2,A′, as a function of K, where the population has been corrected for the degeneracy 2J + 1 of the spin-orbit state (2J + 1 = 2K + 2 for F_1 and 2J + 1 = 2K for F_2).

The figure shows that the F_1 and F_2 states are almost equally populated. The statistical partition seems to be reasonable since the reactants have J=1/2 due to the electron spin of H and the products have J=3/2 or 1/2 due to the spin-orbit coupling in OH. The constraints $\Delta J=1$ or 0 can easily be fulfilled since H_2O and D_2O have distribution of rotational angular momentum over wide range of J.

A-9. Population over the Λ-doublet levels

Fig. 20 shows the ratio of populations in two Λ-doublet levels (F_1A' and F_1A''). The ratio is close to unity at K = 1 and increases with K. The value $A'/A'' = 2.9 \pm 0.5$ at K = 6 is comparable with the value of 3.2 ± 1.0 at K = 11 given by Kleinermanns and Wolfrum at the center of mass translational energy of 250 and 200 kJ/mol [5]. Both results indicate a preference for the A′ component.

In lower rotational levels, the OH molecule rotates with preccession. Since the axis of rotation is determined by a vector sum of angular momenta of rotation, spin and orbital, it is not perpendicular to the molecular axis. Hence the electron lobe tends to direct randomly with respect to the plane of rotation for lower K. This situation may lead to an "apparent" statistical distribution (1:1) over the Λ-doublet components. However, for higher levels, the direction of the unpaired electron lobe can be defined uniquely with respect to the plane

of rotation.

On the basis of a simple dissociation model from the transition state, Bronikowski and Zare predicted the A′/A" ratio for the bimolecular reaction A+BC→AB+C in the large K limit [33]. They assumed the followings,

[1] the motion of A in the transition state [ABC] determines the plane of rotation of AB.

[2] the unpaired π orbital lying along the BC bond may be resolved into a projection onto the AB plane of rotation and perpendicular to this plane, which correlate with $\Pi(A')$ and $\Pi(A")$, respectively.

[3] there is no preferred geometry for dissociation of [ABC].

With these assumptions, they anticipated that the ratio of Λ-doublet populations is

$$A'/A" = 2 \qquad (22).$$

The bending motion on saddle point would determine the plane of rotation of OH" so as to cause the rotation in the H′OH" plane. Therefore, the assumption of rotational excitation through the bending vibration would lead to a preferred population of the A′ component, because the unpaired electon exist in the rotational plane of OH at the time of bond breaking. Our result of A′/A"=2.9±0.5 at K=6 may be the result of this dynamical preference.

A-10. Surprisal analysis

According to the procedure of Levine and Bernstein [34], we performed the surprisal analysis for the rotational distribution of OH produced in the $H+H_2O$ reaction under the bulk condition. Assuming that all energetically accessible quantum states are occupied statistically, the prior distribution for individual rovibrational state of $OH(X^2\Pi)$ with total available energy, E, is given by

$$P^0(v'',J'')=(2J+1)\int_{E_I=0}^{E-[E_V(OH)+E_J(OH)]} \rho[E_I(H_2)]\rho(E_T)dE_I/P(E) \qquad (23)$$

where $E_T=E-[E_V(OH)+E_J(OH)]-E_I(H_2)$. The internal state densities for OH and H_2 are designated by $(2J+1)$ and $\rho[E_I(H_2)]$, respectively. The translational state density is designated by $\rho_T(E_T)$. The factor $\rho(E)$ is the total state density of products at given available energy E and is given by

$$\rho(E)=\sum_{\substack{v''J''=0\\=0}}^{v^*J^*}\sum(2J''+1)\int_{E_I=0}^{E-[E_V(OH)+E_J(OH)]} \rho[E_I(H_2)]\rho(E_T)dE_I \qquad (24)$$

where $J^*(v)$ is the highest energetically permitted value of J^* and v^* is that of v" for a given total available energy. The translational state density is proportional to $E_T^{1/2}$ by the phase space theory. If we assume a rigid rotor model for H_2, the internal state density of H_2 is given by

$$\rho[E_I(H_2)]=\{E-E_V(OH)+E_J(OH)]-E_T\}^{1/2}$$
$$=E_I^{1/2} \qquad (25)$$

Therefore, the inner integral of equations (23) and (25) is given by

$$\int_{E_I=0}^{E-\{E_V(OH)+E_J(OH)\}} E_I^{1/2}(E-[E_V(OH)+E_J(OH)]-E_I\}^{1/2}dE_I$$

This integral is of the form $\int_0^A (X)^{1/2}(A-X)^{1/2}dX$ which is transformed to a beta function yielding integral to give $[A\Gamma(3/2)]^2/\Gamma(3/2+3/2)=\Pi(A^2)/8$. Therefore, the final form of equations (23) and (24) is given by

$$P^0(v'',J'')=(2J''+1)[E-E_V(OH)-E_J(OH)]^2/\rho(E) \qquad (23)'$$

and

$$P(E)=\int_{v''J''=0}^{v^*J^*(v^*)} (2J''+1)[E-E_V(OH)-E_J(OH)]^2dJdv \qquad (24)'$$
$$=0$$

Using equations (23)' and (24)', we obtain the prior distribution over the energetically possible OH rotational state in this reaction. For the energies of the vibrational and rotational states of OH, we used the calculated value by Dieke and Crosswhite [19].

Fig. 21(a) represents experimental and prior distributions. Experimental distribution is for the v"=0, F_1A' manifold. The figure includes also the distribution calculated by the

quasiclassical trajectory calculation at the center-of-mass translational energy of 250 kJ/mol [7]. In spite of the difference of 90 kJ/mol in the energy of reactants, two rotational distributions are almost the same except for lower K.

The experimental distribution is considerably different from the prior distribution. This suggests that the energy partition for the OH rotation during the reaction is not statistical. The rotational surprisal, $I(v",J)=-\ln[P(v",J)/P^0(v",J)]$, is calculated and shown in Fig. 21(b). Here, $P(v",J)$ and $P^0(v",J)$ represent the experimental and prior rotational distributions, respectively. The rotational distribution obtained under the bulk condition could be characterized by a single "linear surprisal parameter", Θ_R=13.3, as shown in Fig. 21 (b). Θ_R is the slope of $\ln[P(v",J)/P^0(v",J)]$ vs g_r, where g_r is the fraction of available energy in the OH rotation. This surprisal plot can be interpreted as the result of a dynamical restriction on the OH rotational population. For the direct mechanism, especially in the case of a spectator-stripping type mechanism, the collision time is very short, typically, $<10^{-13}$ sec [35], for which the activated complex cannot distribute the energy over all degrees of freedom. In other words, the system cannot erase the memory of the initial conditions.

A-11. $H+H_2O$ reaction under the reactant-pair condition

Reactant-pair reaction (2) has also been studied under the supersonic free jet condition for the purpose of studying the orientational effect in bimolecular reaction, $H+H_2O \rightarrow OH+H_2$.

Structural information of weakly bound complexes is very important in discussing the reaction dynamics in this type of reactions. Unfortunately, the geometric information for the $HBr \cdot H_2O$ complex is not available. Structual information for $HX \cdot H_2O$ (X=F and Cl) by the ab initio calculation [9] and the microwave spectroscopy [8] under the molecular beam condition enable us to estimate the structure of the $HBr \cdot H_2O$ complex.

Fig. 1 shows the structures of two stable isomers of $HBr \cdot H_2O$ determined by the ab initio calculation [9]; namely, the H atom in HBr is bonded to oxygen in H_2O and Br is bonded to oxygen, respectively, as shown in Fig. 1 (a) and (b). Here H_2O lies in the X-Z plane while O-H-Br lies in the Y-Z plane for both conformations. The calculation suggests that the $H_2O \cdots HBr$ is more stable than $HBr \cdots OH_2$ by 16.2 kJ/mol [9]. On the other hand, the theoretical treatment suggests $HX \cdot H_2O$ (X=F and Cl) to have a single conformation; namely, the H atom in HX is bonded to oxygen in H_2O [9]. The microwave spectroscopic measurements have supported this conclusion [8].

Fig. 22 shows the R_{11}-transition in the LIF spectrum of the (0,0) band of OH produced in the photodissociation of $HBr \cdot H_2O$. Unfortunately, we could not obtain any spectrum from which a

reliable estimation on the rotational population can be made, since the signal intensity decreases rather rapidly during a scan. This is presumably due to some chemical reactions occurring in the nozzle. The LIF signals were weak in comparison with those in the $H+N_2O$ reaction under the reactant-pair condition (see below) and non-observation of the parent complex ion signal in the mass spectrometric measurements make it uncertain if the spectrum shown in Fig. 22 arise from the reactant-pair reaction (2).

The results for a similar bimolecular reaction, $H+CO_2$, under the reactant-pair condition [36] would give us a useful information. Fig. 23 shows two types of conformations of the $CO_2 \cdot HBr$ complex determined by theoretical calculations by Wittig et al. [32], In one of them, the Br-C line is perpendicular to the CO_2 axis, with the H-Br bond axis parallel to the CO_2 axis (type (1)), while, in the other, $HBr-CO_2$ is nearly linear, with hydrogen-bonded to the oxygen in CO_2 (type (2)). Up to now, only the type (1) conformer has been confirmed by the IR spectroscopic measurements.

Although we may expect that the reactant-pair reaction in $HBr \cdot CO_2$ occurs from the type (2) conformation, Wittig et al. have suggested that it occurs from the type (1) conformation because of the effect of internal motion in the complex [36]. They have insisted that the reaction from the type (2) conformation cannot occur because the hot hydrogen cannot acquire significant kinetic

energy; namely, the hydrogen atom reacts with the O atom in CO_2 before the HBr bond completely breaks. On the other hand, the hot hydrogen in the type (1) conformation reacts with O by the large-amplitude bending motion in the Br-CO_2 plane.

In the case of the H+H_2O reaction under the reactant-pair condition, we expect that the reactant-pair reaction (2) occurs by the conformation of type (1) as shown in Fig. 1. The type (2) comformation would hardly give OH upon optical bond scission of H-Br.

However, the reaction cross section for the type (1) conformation may be low in view of the favorable direct abstraction mechanism discussed above for the bimolecular reaction. Since the result for the bimolecular reaction seems to exclude the existence of intermediate of the type H_3O, there might be no efficient channel to produce H_2 and OH from the type (1) conformation. Therefore, the difficulty we met in measuring the reliable LIF spectra may partly be due to this essential reason. The cross section in this case, if any, would arise from the coupling of the Br-H-O vibrations and other vibrational modes such as bending motions.

B. The $O(^3P_J)$ + H_2S reaction under the bulk condition

B-1. Energetic

In comparison with the study of channel (4) [37], there is little information on reaction (3). The internal state distribution has been reported by Agrawalla and Setser for OH produced by reaction (3) under the bulk condition [38]. They found the activation barrier to be 26.0 ± 4.2 kJ/mol.

B-2. Examination of experimental condition for bulk experiments

NO_2 and H_2S may undergo the following reactions;

$$NO_2 + H_2S \rightarrow H_2O + NO + S \quad (26)$$

$$H_2O + NO_2 + NO \leftrightarrow 2HNO_2 \quad (27)$$

Nitrous acid is known to produce OH by the 355 nm photodissociation, which would disturb the measurement of reaction (3). To confirm that the reaction (27) is minor in the present experimental condition, we have measured mass spectra with a quadrupole mass spectrometer (SHIMAZU CONCEPT-QP). The sample gas was prepared by mixing NO_2 and H_2S in a 1:1 ratio at the total pressure of 40 Torr. The measurement of mass spectra was performed in a long time scale of 10-60 min. Results are shown in Fig. 24. Although the energy of electron impact is relatively low, possibility of the dissociative ionization can not be excluded. Nevertheless, it is concluded that reaction

(27) occurs very slowly and would not proceed appreciably in the time scale of the LIF experiment, where the sample is completely pumped out before the next laser shot, namely, within 0.1 sec.

The LIF spectra of OH produced in the photodissociation of HNO_2 at 355 nm [39] shows that the LIF intensity for the R_{22} branch is abnormally more intense than that for the P_{11} branch. On the other hand, the present result shows a normal intensity ratio. Therefore, we conclude that the present result is exclusively due to reaction (3).

In comparison with the $H+H_2O$ case, the present experiments were performed under a relatively low total gas pressure of 10-15 mTorr. Therefore, we convince that the rotational relaxation does not occur.

Relaxation of electronically excited $OH(A^2\Sigma^+)$ due to the reaction with H_2S (or NO_2);

$$OH(A^2\Sigma^+) + H_2S \text{ (or } NO_2) \rightarrow OH(X^2\Pi) + H_2S \text{ (or } NO_2) \quad (28)$$

may occur in view of their large (0.89D and 0.29D, respectively, for H_2S and NO_2 [25]) dipole moments. The correction for the relaxation was not performed in this case because no data is available.

B-3. LIF spectra and rotational distribution of OH

Fig. 25 shows a part of the (0,0) band in the LIF spectrum of OH taken under a typical experimental condition (the total

pressure and the pump-probe delay time are 10 mTorr and 200 nsec, respectively). The observed band can be assigned entirely to OH.

Fig. 26 shows the rotational state distribution of OH(v"=0) for the F_1A', F_2A' and $F_1A"$ manifolds obtained from the analysis of the R_{11}-, R_{22}- and Q_{11}-branches, respectively. In the case of the F_1A' and F_2A' states, the rotational distribution is peaked at K=2 and falls to zero at K=6. On the other hand, in the case of the $F_1A"$ state, the rotational distribution is peaked at K=3 and falls to zero at K=6.

Fig. 27 shows a Boltzmann plot of the data shown in Fig. 26. It shows that the distributions are of Boltzmann type, with the rotational temperatures of 370 ± 60 and 260 ± 50 K for the F_1A' (or F_2A') and $F_1A"$ manifolds, respectively. These rotational temperatures correspond to the energies of about 4 and 3 %, respectively, of the available energy of 76 kJ/mol. Here, the available energy is given by $E_{AVL}=E_{TRANS}+E_{INT}-\Delta H_0$, where E_{TRANS} is the translational energy of the reactants, E_{INT} is the rotational and vibrational energy of H_2S and ΔH_0 is the enthalpy change. ΔH_0 is calculated to be 43 kJ/mol [40]. E_{TRANS} is estimated to be 23 KJ/mol in section (2.B). Also, $E_{INT}=(3/2)RT(rotation)+3RT(vibration)=11$ kJ/mol at room temperature. Therefore, we obtain $E_{AVL}=76$ kJ/mol.

B-4. Reaction mechanism

The low rotational excitation of OH is similar to the

reaction of $O(^3P)$ with organic molecules (for example, $C(CH_3)_4$, C_6H_{12} and $(CH_3)_3CH$) [41]). In these reactions, OH formed in the reaction has a cold rotational distribution, which is rationalized in terms of a strong dynamical preference for direct hydrogen atom abstraction via tightly collinear configuration. We expect a similar mechanism for the $O(^3P)$ + H_2S reaction. If reaction (3) proceeds through collinear intermediates (O-H-S-), the repulsion between O-H and S (or SH) excites only the translation and vibration of OH with little excitation of rotation. On the other hand, if the reaction occurs principally through bent configurations, repulsion between O-H and S (or SH) produces a torque in OH and causes substantial rotational excitation. We therefore conclude that this reaction occurs preferentially when $O(^3P)$ approaches to one of the S-H bond to form a linear transition state.

B-5. Population over the spin-orbit components

Fig. 28 shows the ratio of populations in two spin-orbit components F_1A' and F_2A' as a function of K, where the population has been corrected for the degeneracy 2J+1 of the spin-orbit state (2J+1 = 2K+2 for F_1 and 2J+1 = 2K for F_2). The figure shows that the F_1 and F_2 states are almost equally populated. The spin-orbit population ratio was measured recently, for $O(^3P_J)$ produced by the photodissociation of NO_2 at 355 nm, indicating that the distribution is statistical [13]. Therefore, we assume

that the available energy released in the NO_2 dissociation is distributed statistically over the $O(^3P_{2,1,0})$ spin-orbit states. Assuming Boltzmann distribution, the population may be expressed by the following equation,

$$P \propto (2J+1)\exp(-\Delta\varepsilon/RT) \tag{29}$$

where $\Delta\varepsilon=(1/2)\varepsilon_0 J(J+1)$. The population ratio between the components should be

$$P(^3P_2):P(^3P_1):P(^3P_0)=5:3\alpha^2:\alpha^3 \tag{30}$$

where $\alpha=\exp(-\varepsilon_0/RT)$. We assume that the $O(^3P_J)$+ H_2S reaction with different J=2,1,0 proceeds via different surfaces determined by the conservation of total angular momentum; i.e., $O(^3P_2)$ correlates with $OH(^2\Pi_{3/2})$ through a $^3\Pi_2$ surface, while $O(^3P_0)$ correlates with $OH(^2\Pi_{1/2})$ through a $^3\Pi_0$ surface. On the other hand, $O(^3P_1)$ gives rise to a nonreactive $^3\Sigma$ surface which does not correlate with $OH(^2\Pi_{3/2,1/2})$ [41]. Fig. 29 shows the schematic correlation diagram drawn under the assumption of (O-H-S-) linear transition state, and treating SH' as a spherical particle.

The correlation has been drawn on the basis of the fact that the vector sum of spin and orbital momentum, namely, the total angular momentum must be conserved in the adiabatic limit. The energy of $O(^3P_0)$ is higher than $O(^3P_2)$ by about 2.8 kJ/mol [41]. If this reaction is completely adiabatic, $O(^3P_2)$ and $O(^3P_0)$ are

correlated to F_1 and F_2 levels of OH, respectively.

Therefore $F_1/F_2=5/\alpha^3$ and even if $T\rightarrow\infty$, $F_1/F_2=5$. If the temperature is common, the ratio of population in two spin-orbit components of OH, $F_1K/F_2(K+1)$, should be 5/2=2.5 for K=1 and approaches 5 for $K\rightarrow\infty$.

On the other hand, if the reaction is completely diabatic, there is no memory of the initial distribution of $O(^3P)$ spin-orbit states; i.e., the spin-orbit population ratio should be 1. The ratio of the sums of the F_1 and F_2 state populations in the present result amounts to 1.1 ± 0.3, suggesting that this reaction proceeds via diabatic surfaces.

The non-conservation of angular momentum is not striking in this case, since, even if the O-H-S bond is linear, we can never ignore the effect of the other S-H bond. Then the activated complex has no orbital degeneracy at all and it seems to be natural that the angular momentum is not conserved.

B-6. Population over the Λ-doublet levels

Fig. 30 shows the ratio of populations in two Λ-doublet levels (F_1A' and F_1A''), which indicates a preference for the A′ component. The ratio is close to unity at K=1 and increases with K to A′/A″=2.2 ± 0.2 at K=5. If we assume the linear or nearly linear activated complex as discussed above, the plane of rotation of OH may be determined by the direction of attack of $O(^3P)$. If there is no preference of reaction cross section with

respect to the direction of attack, the plane of rotation would be randomly oriented. In addition, the direction of the unpaired electron lobe centered on the attacking O atom cannot be specified except for that it should lie in the plane perpendicular to the O-H axis. These situations may result in a "random" distribution over the Λ-doublet states.

Our experimental result of A′/A"=2.2±0.2 is indeed close to the "prior" value predicted by Bronikowski and Zare [33] (see section (3-A-10)). However it is not certain if their model could be applied to this case, where the oxygen atom attacks and takes the hydrogen atom to form OH. The situation would be much different from the case treated by Brownikowski and Zare.

B-7. Suprisal analysis

We performed the surprisal analysis for the rotational distribution in a similar manner to the $H+H_2O$ reaction. Fig. 31 (a) represents experimental and prior distributions. The experimental distribution is shown for the v"=0, F_1A' manifold. Two rotational distributions are different considerably. Rotational surprisal, $I(v",J)=-\ln[P(v",J)/P^0(v",J)]$ was obtained by using the results of Fig. 31(a), where $P(v",J)$ and $P^0(v",J)$ represent the experimental and prior distribution, respectively. The rotational distribution can be characterized by a single "linear surprisal" with $\theta_R=25.0$ as shown in Fig. 31(b). This value is about two times larger than that for the $H+H_2O$ reaction,

indicating that the experimental distribution for the $O+H_2S$ reaction is more deviated from the prior distribution than that for the $H+H_2O$ reaction. It is therefore suggested that the kinematic constraint should exist in this case, compared with the direct hydrogen-abstraction reaction (1).

C. The H + N_2O reaction under the reactant-pair condition

Schematic potential surfaces [14] are given in Fig. 2 for the $H+N_2O \rightarrow OH+N_2$ reaction (5). Two channels correspond to the attacks of the hydrogen atom to the oxygen end and to the nitrogen end of N_2O:

$$H + NNO \rightarrow H\cdots NNO \rightarrow OH + N_2 \qquad (31\text{-A})$$

and

$$H + ONN \rightarrow H\cdots ONN \rightarrow OH + N_2 \qquad (31\text{-B})$$

Dissociation of HI at 248 nm yields the I atom in two spin-orbit states, $I(^2P_{3/2})$ and $I^*(^2P_{1/2})$, in the ratio of 0.75:1 [6], which differ in energy by about 92 kJ/mol. These two dissociation channels give rise to two different center-of-mass H atom energies, 183 and 96 kJ/mol, respectively. Both energies exceed the barriers corresponding to (31-A) and (31-B). Therefore, the OH product rotational distribution may be a sum of contributions from these channels.

N_2O could be photolyzed at 248 nm to produce $N_2+O(^1D_2)$ on the energetical basis [18]. $O(^1D)$ is known to react with HI [18] as

$$N_2O\cdot HI + (h\nu=248\ nm) \rightarrow (O + HI) + NO \rightarrow OH + I + NO \qquad (32).$$

Hoffman et al. have suggested that this reaction does not contribute significantly to the OH production in the case of the reactant-pair reaction of $HBr\cdot N_2O$ [42]. Accordingly, we ignore

the effect of reaction (32) in the following discussion.

Structural information of weakly bound complexes is very important in discussing the mechanism of reactions under the reactant-pair condition. Although the structure of the $HI \cdot N_2O$ complex has not been determined experimentally, structural information for $HX \cdot N_2O$ (X=F,Cl and Br) by ab initio calculations [15] and the infrared and microwave spectroscopic experiments [43] under the molecular beam condition enables us to estimate the structure.

Fig. 3 shows the structure of three stable isomers of $HCl \cdot N_2O$, type (1), (2) and (3), determined by an ab initio calculation [15]. In the case of $HF \cdot N_2O$, the infrared and microwave spectroscopic measurements were performed [43], indicating existence of two isomers, namely, the linear isomer FH···NNO and the bent isomer NNO···HF. Both isomers correspond to types (3) and (2), respectively, in Fig. 3. The IR spectroscopic measurements have revealed only the bent isomer NNO···HX for $HCl \cdot N_2O$ and $HBr \cdot N_2O$ [43]. However, we cannot exclude the existence of other two isomers, types (1) and (2), predicted theoretically.

Although we employ the molecular beam condition, there is a possibility of bimolecular collisions of N_2O with H produced by irradiation of free HI during the supersonic expansion. This possibility can be excluded on the following basis. The dependence of the OH LIF signal on the delay between the

photolysis and probe lasers was measured in the nozzle expansion over the range of 0.1 - 1.0 μsec, as shown in Fig. 32. It was obtained by monitoring the LIF signal for OH, v"=0, K=7. Similar results were obtained for other v"=0 rotational levels. No increase of signal is observed with increasing the delay time, suggesting that no measurable rise time exists under the reactant-pair condition. This is what expected for a rapid unimolecular decomposition of the complex, and is in clear contrast to the bimolecular reaction which shows a rise time associated with a flight time of H toward N_2O.

OH may also be produced from higher order complexes other than $HI{\cdot}N_2O$. To examine this contribution, the relative abundance of the cluster species was measured by mass spectrometry. Fig. 33 shows a time profile of $(HI)_n{\cdot}(N_2O)_m$ clusters. The horizontal axis shows the delay between the time of valve opening and the signal detection. The ion intensity of each species has been normalized. The cluster species appear after a significant delay from the rise of the monomer signal with a shorter duration. The delay is also dependent on the cluster size (e.g., $HI{\cdot}(N_2O)_2$ signal appears after $(HI)_2$), indicating that it is not only due to the difference of velocity but also to the delayed formation of higher-order cluster species during the expansion.

The time profile of the LIF signal of the monomer fluorescent species such as NO_2 followed the jet pulse, whereas the OH signal from the present reaction appears only in the last

1/3 of the jet pulse. On the other hand, the dependence of the OH LIF signal on the delay between the injector and photolysis laser pulse was measured in the $HI{\cdot}N_2O$ jet experiment over the range of 0.1-1.0 μsec, as shown in Fig. 34, which was obtained by monitoring the LIF signal for OH (v"=0, K=7).

Comparing Fig. 33 and 34, the half width at half maximum (HWHM) of the $HI{\cdot}N_2O^+$ mass signal and the OH LIF signal are found to be about 140 and 110 μsec, respectively. These two values seem to be in good agreement with each other if we take account of the flight time for the former. The delay time of 840 μsec employed for the delay between the injector and photolysis laser pulses corresponds to the early stage of the rise of the LIF signal (Fig. 34), where the production of higher-order clusters is not significant (Fig. 33).

Fig. 35 shows a part of the OH (v"=0) LIF spectrum due to the $A^2\Sigma^+ \leftarrow X^2\Pi$ transition for the $H+N_2O$ reaction under the reactant-pair condition. The stagnation pressure and the mixture ratio are 2.5 atm and $HI:N_2O:He=2.6:4.4:93$, respectively. Delay time between both lasers is 200 nsec. The distance between the nozzle position and the laser crossing area is 3 cm.

Hollingsworth et al. have reported the rotational distribution of OH produced in the $H+N_2O$ reaction under the bulk condition. They have employed the total gas pressure and the pump-probe delay time are 100 mTorr (in the 1:1 ratio of HI and N_2O) and 500 nsec, respectively [16]. Hot hydrogens were

produced by the photodissociation of HI at 248 nm. Their results suggest that the rotational distribution of OH is a superposition of two Boltzmann distributions characterized by the rotational temperatures of 1100 ± 100 and 4700 ± 300 K as shown in Fig. 36.

The reactant-pair reaction studied here also shows a dual Boltzmann distribution as shown in Fig. 37. It shows the rotational distributions in the F_1A' and F_2A' manifolds of OH obtained from the R_{11}, R_{22}-branches. The rotational temperatures for the two components are 600±100 and 3800±400 K, which are colder than the corresponding temperatures for the bulk reaction [16].

Let us assume for the moment that only the bent isomer NNO···HI exists (type (2) in Fig. 3). For this conformation, the hydrogen atoms attack the oxygen end of N_2O, corresponding to the "direct" channel shown in Fig. 2. Two components in the Boltzmann distribution should then be attributed to the contribution from the I and I^* channels with different translational energies of hot hydrogen atoms. Since the cross sections of photodissociation for both channels are almost the same (0.75:1 [6]), both channels may contribute almost equally to this reaction (8).

This reaction channel (5) has a large exoergicity of about 263 kJ/mol. Both rotational temperatures of 3800 and 600 K correspond to the rotational energies of 445.9 KJ/mol and 358.9KJ/mol, respectively, which are 7.1 and 1.4 %, respectively,

of the available energies (for the I channel and the I^* channel). If the initial energy of reactants is statistically partitioned into the whole degrees of freedom of the products, the fraction of energy partitioned into rotation is

$$g_r = (\text{OH rotational degrees of freedom})/[(\text{relative translational degrees of freedom between OH and } N_2) + (N_2 \text{ rovibrational degrees of freedom}) + (\text{OH rovibrational degrees of freedom})]$$
$$= RT/((3/2)RT + 2RT + 2RT) \qquad (33)$$
$$= 18\%$$

Experimental fractions, 7.1% and 1.4% corresponding to the I and I^* channels, respectively, are lower than the value estimated on the assumption of equipartition.

For the I and I^* channels, excess energies on the saddle point in the "direct" channel are 104 and 17 KJ/mol, respectively. The ratio is 104/17=6.1. On the other hand, the ratio of rotational temperatures for two distributions is 3800K/600K=6.3. This is in good agreement with the ratio of excess energies. This coincidence may suggest that the rotational excitation of OH is almost exclusively determined by the excess energy above the barrier, while the energy released after the barrier does not contribute to the rotational excitation. In other words, the initial memory contained in the complex is well retained beyond the activation barrier.

Our experimental results seem to be well explained by the assumption of the existence of only one isomer, namely, the bent isomer NNO···HI (type (2) as shown in Fig. 3), However, there is no experimental evidence to exclude the existence of other isomers. More detailed studies are required to clarify this point; i.e., the dependence on stagnation pressure and the structure determination by the IR (microwave) spectroscopic measurements.

4. Conclusions

A. The H + H_2O reaction under the bulk and reactant-pair conditions

The elementary reaction, H + H_2O → OH + H_2, has been studied under the bulk and reactant-pair conditions. The OH radical produced in the above reaction with the hot hydrogen atom produced by the photolysis of HX (X=Br and I) is monitored by the LIF technique. The results of the bimolecular reaction indicates that the nascent rotational distribution of OH is of Boltzmann type with a remarkably non-statistical partition over the Λ-doublet sublevels, while the spin-orbit components are populated statistically. It is suggested that the rotational excitation of OH does not depend on the collision energy of hot hydrogen by comparing the present and Kleinermanns and Wolfrum's works. The bimolecular reaction $H+H_2O \rightarrow OH+H_2$ is suggested to proceed by the direct mechanism without any long-lived intermediate, on the basis of the heavy water experiment together with the prediction by ab initio calculations. Moreover, the non-excitation of vibrational mode, which may be understood as the result of a later barrier in the reaction coordinate, together with the inefficient rotational excitation, seem to be in favor of a spectator-stripping type mechanism applicable to this reaction. The model is presented in which the bending mode of the activated complex play a role in transferring the energy to the OH

rotation. This seems to account for the insensitivity of rotational temperature to the excess energy.

Photochemical reaction of weakly-bound complex, $HBr \cdot H_2O$ has been studied in a supersonic jet. Preliminary LIF spectra have been obtained for the OH radical produced by the photolysis of the complex at 193 nm. Though it is not conclusive, the observation of OH in this reaction may indicate a role of the out-of-axis vibrational motion of H in the complex, since the direct attack of H to oxygen may be inefficient in view of the direct mechanism established in the bimolecular reaction.

For further studies, it would be interesting to monitor the internal state distribution of the other product H_2 by using REMPI or LIF method. This information would provide more detailed information on the reaction mechanism.

B. The $O(^3P_J)$ + H_2S reaction under the bulk condition

Elementary reaction, $O(^3P) + H_2S \rightarrow OH + HS$, has been studied under the bulk condition. The OH radical is monitored by the LIF technique. The nascent distribution of OH is of Boltzmann type with an extremely low rotational temperature. This result would indicate that the reaction proceeds through the collinear configuration on the saddle point. Distributions over the spin-orbit component are non-statistical, which indicates that the reaction proceeds through the diabatic surfaces with a slightly bent configration at the saddle point. The ratio of both Λ-

doublet levels indicates A'/A"=2, which is in good agreement with the statistical value predicted by Broniskowsky and Zare.

For further studies, it would be interesting to measure the rotational distribution of the other product, the HS radical, which would be helpful in discussing the angular momentum constraints for the fine structure distribution in more detail.

C. The H + N_2O reaction under the reactant-pair condition

Photochemical reaction of weakly-bound complex, $HI \cdot N_2O$ has been studied under the reactant-pair condition. The OH radical produced by the 248 nm irradiation is monitored by the LIF technique. The rotational distribution is represented by two Boltzmann distributions. Results indicated that the rotational temperature of product OH under the reactant-pair condition is slightly colder than that for the bulk condition. It is shown that the present results can be explained in terms of the existence of only one comformer (type (2) in Fig. 3). But we can not exclude that the existence of another comformers (type (1) and (3) in Fig. 3).

For further studies, it would be interesting to measure the internal states distribution of NH. For the $HBr \cdot N_2O$ complex at 193 nm photolysis, $NH(X^3\Sigma)$ rotational distribution has been obtained [42]. Although the $HI \cdot N_2O$ system studied at 266 nm has no excess energy available for the NH formation [14], the 248 nm

irradiation of $HI{\cdot}N_2O$ has sufficient excess energy for the NH formation. It is interesting to compare the rotational state distributions of NH produced from the $HBr{\cdot}N_2O$ and $HI{\cdot}N_2O$ systems.

5. Acknowledgments

This study was accomplished in collaboration with Prof. Ichiro Hanazaki at the Institute for Molecular Science. The author wishes to express his gratitude to Prof. Hanazaki for his kind and continuous encouragement in carring out the research. The author also wishes to express his gratitude to Dr. Teruhiko Nishiya and Dr. Masao Takayanagi for their kind and helpful suggestions in carrying out the research. The author wishes to thank Dr. Hiroshi Ohoyama of Osaka University for his valuable suggestion during the research.

6.Reference

[1] S. Stolte, Ber. Bunsenges, Phys. Chem. 86 (1982) 413.

[2] G. Radhakrishnan, S. Buelow, and C. Wittig, J. Chem. Phys. 84 (1986) 727.

[3] D. Yaron, K. I. Peterson, D. Zolandz, and W. Klemperer and F. J. Lovas and R. D. Suenram, J. Chem. Phys., 92 (1990) 7095.

[4] V. N. Kondratiev, Comprensive chemical kinetics, Vol. 2. eds. C. H. Banford and C. F. H. Tipper (Elsevier. Amsterdam. 1969) p.118.

(a) K. Kleinermanns and J. Wolfrum, Appl. Phys. B 34 (1984) 5.

[6] (a) R. D. Clear, S. J. Riley and K. R. Wilson, J. Chem. Phys . 63 (1975) 1340.

(b) L. E. Compton and R. M. Martin, J. Phys. Chem. 78 (1969) 3474.

(c) Y. Matsumi, K. Tonokura and M. Kawasaki, J. Chem. Phys. 93 (1990) 7981.

[7] (a) H. Elgersma and G. C. Schatz, Inter. J. Quantum. Chem. Symposium. 15 (1981) 511.

(b) G. C. Schatz, M.C. Colton and J. L. Grant,J. Phys. Chem. 88 (1984) 2971.

[8] A. C. Legon and L. C. Willouughby, Chem. Phys. Lett. 95 (1983) 449.

Z. Kisiel, A. C. Legon and D. J. Millen, Proc. R. Soc.

Lond. A 381 (1982) 419.

[9] Y. Hannachi, B.Silvi, J. P. Perchard and Y. Bouteiller, Chem. Phys. 154 (1991) 23.

[10] D. L. Singleton, R. S. Irwin,W. S. Nip and R.J.Cvetanovic, J. Phys. Chem. 83 (1979) 2195.

D. L. Singleton, G. Paraskevopoulos and R. S. Irwin, J. Phys. Chem. 86 (1982) 2605.

[11] K. G. McKendrick, D. J. Rakestraw and R. N. Zare, Faraday Discuss. Cnem. Soc. 84 (1987) 39.

R. Zhang, W. j. van der Zande, M. J. Bronikowski and R. N. Zare, J. Chem. Phys. 94. (1991) 2704.

[12] E. Pollak, J. Chem. Phys. 78 (1983) 1228.

[13] H. -G. Rubahn, W. J. van der Zande, R. Zhang, M. J. Bronikowski and R. N. Zare, Chem. Phys. Lett. 186 (1991) 154.

[14] P. Marshall and A. Fontijn, J. Chem. Phys. 86 (1987) 5540.

[15] D. J. Pauley, M. A. Roehrig, L. Adamowicz, J. C. Shea, S. T. Haubrich and S. G. Kukolich, J. Chem. Phys. 94 (1991) 899.

[16] W. E. Hollingsworth, J. Subbiah and G. W. Flynn and R, E. Weston, Jr, J. Chem. Phys. 82 (1985) 2295.

[17] H. Ohoyama, M. Takayanagi, T. Nishiya and I. Hanazaki, Chem. Phys. Lett. 162 (1989) 1.

[18] H. Okabe, Photochemicary of small molecules (A Wiley-Interscience publication).

[19] G. H. Dieke and M. Crosswhite, J. Quant. Spectrosc. Radiat. Transfer. Vol. 2 (1961) 97.

[20] G. Herzberg, Molecular spectra and molecular structure, Vol. 1. Spectra of diatomic molecules (Van Nostrand, Princeton, 1950).

[21] M. H. Alexander et al., J. Chem. Phys. 89 (1988) 1749.

[22] W.L.Dimpel and J.L.Kinsey, J. Quant. Spectrosc. Radiat. Transfer. Vol. 21 (1979) 233.

[23] M. A. A. Clyne, J. A. Coxon and A. R. W. Fat, J. Mol. Spectroscopy. 46 (1973) 146.

[24] C. B. Cleveland and J. R. Wiesenfeld, J. Chem. Phys. 96 (1992) 248.

[25] A. L. McClellan, Tables of Experimental Dipole Moments (W. H. Freeman and Company, San Francissco and London).

[26] private communication.

[27] M. C. Hsiao, A. Shinha and F. F. Crim, J. Phys. Chem. 95 (1991) 8263.

[28] G. C. Schatz and H. Elgersma, Chem. Phys. Lett.73 (1980) 21.

[29] J. H. Collomon, E. Hirota, I. Iijima, K. Kuchitsu and W. J. Lafferty, Structure Data of Free Polyatomic Molecules, Vol . 15. eds. K.-H.Hellwege (Springer-Verlag Berlin Heidlberg New York London Paris Tokyo) p.112.

[30] (a) K. Kleinermanns, E. Linnebach, J. Chem. Phys. 82 (1985) 5012.

(b) M. J. Bronikowski, R. Zhang, D. J. Rakestraw and R. N. Zare, Chem. Phys. Lett. 156 (1989) 7.

(b) K. Kessler and K. Kleinermanns, Chem. Phys. Lett. 190 (1992) 145.

[32] G. Herzberg. Molecular Spectra and Moleclar Structure Vol. 2. Infrared and Raman spectra of Polyatomic Molecules (Va Nostrand Reinhold Company) p.282.

[33] M. J. Bronikowski and R. N. Zare, Chem. Phys, Lett.166 (1990) 5.

[34] R.D.Levine and J.L.Kinsey, Atom-Molecule collisision theory edited by R.B.Bernstein (Plenum press New York and London, 1979), P.693.

[35] R. D. Levine and R. B. Bernstein, Molecular Reaction dynamics, (Oxford University Press, 1976).

[36] S. K. Shin, C. Wittig and W. A. Goddard, J. Phys. Chem. 95 (1991) 8048.

[37] (a) N. Balucani, L. Beneventi, P. Casavecchia, D. Stranges and G, G, Volpi, J. Chem. Phys. 94 (1991) 8611.

(b) Z. Z. Zhu, J. J. W. McDouall, D. J. Smith and R. Grice, Chem. Phys. Lett. 188 (1992) 520.

[38] B. S. Agrawalla and D. W. Setser, J. Chem. Phys . 86 (1987) 5421.

[39] R. Vasudev and R. N. Zare, J. Chem. Phys. 80 (1984) 4863.

[40] D. L. Baulch et al., J. Phys. Chem. Ref. Data, Vol. 11 (1982) 438.

[41] P. Andresen and A. C. Luntz, J. Chem. Phys. 72 (1980) 5842.

[42] G. Hoffmann, D. Oh and C. Wittig, J. Chem. Soc., Faraday Trans. 2. 85 (1989) 1141.

[43] Y. P. Zeng, S. W. Sharpe, D. Reifschneider, C, Wittig and R. A. Beaudet, J. Chem. Phys. 93 (1990) 183.

K	10^{-7} x k	R/R_0
0	2.32	0.5
1	2.35	0.47
2	2.42	0.46
3	2.42	0.46
4	2.32	0.47
5	2.23	0.49
6	2.09	0.51
7	2	0.52
8	1.83	0.55
9	1.67	0.58
10	1.57	0.6
11	1.54	0.61
12	1.51	0.61

Table 1. K dependence of $OH(A^2\Sigma^+)$ quenching rate constants. (k = OH quenching rate constants ($Torr^{-1}s^{-1}$). $R/R_0 = [OH(A^2\Sigma^+)]/[OH(A^2\Sigma^+)]_0$ calculated from equation (18).)

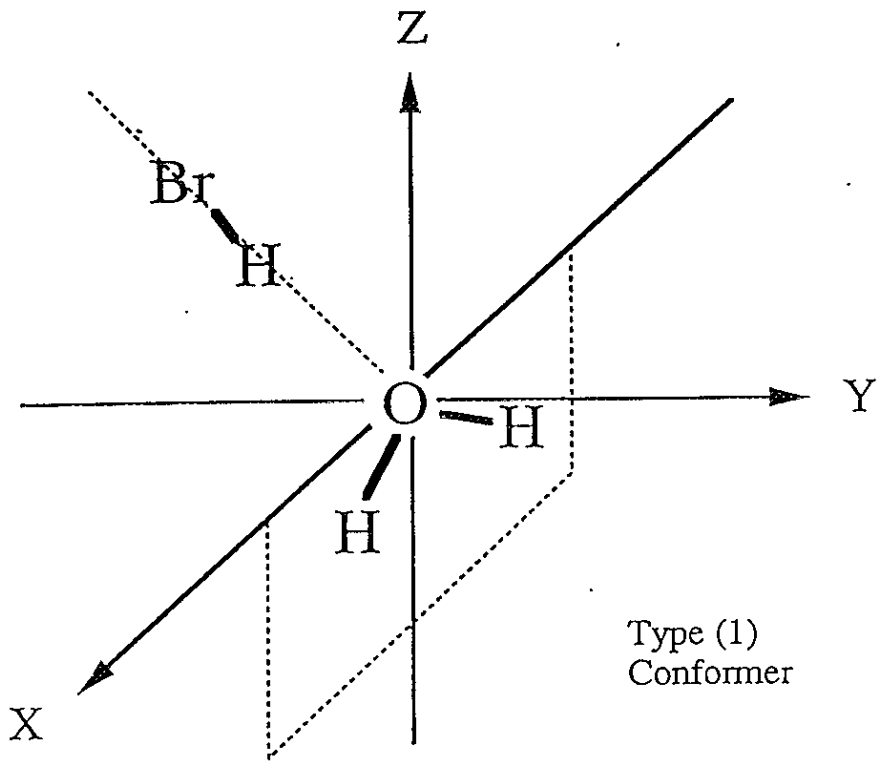

H_2O is located on the X-Z plane.

O-Br-H angle is on the Y-Z plane.

Fig.1(a). Structure of type(1) conformer(H_2O···HBr) of HBr·H_2O complex.

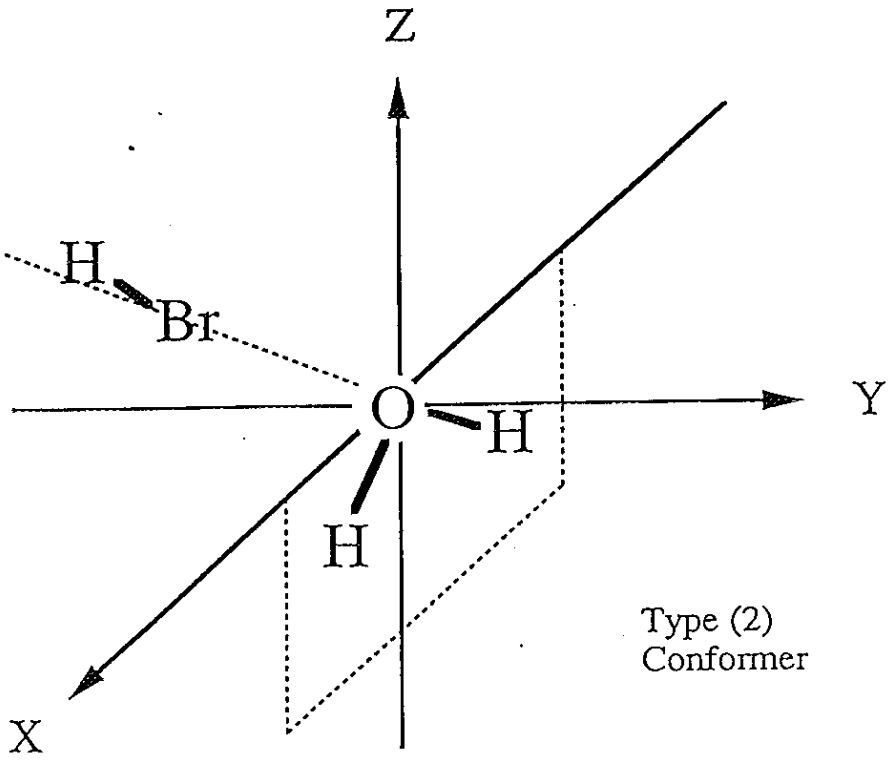

H_2O is located on the X-Z plane.

O-Br-H angle is on the Y-Z plane.

Fig.1(b). Structure of type(2) conformer ($HBr\cdots OH_2$) of $HBr{\cdot}H_2O$ complex.

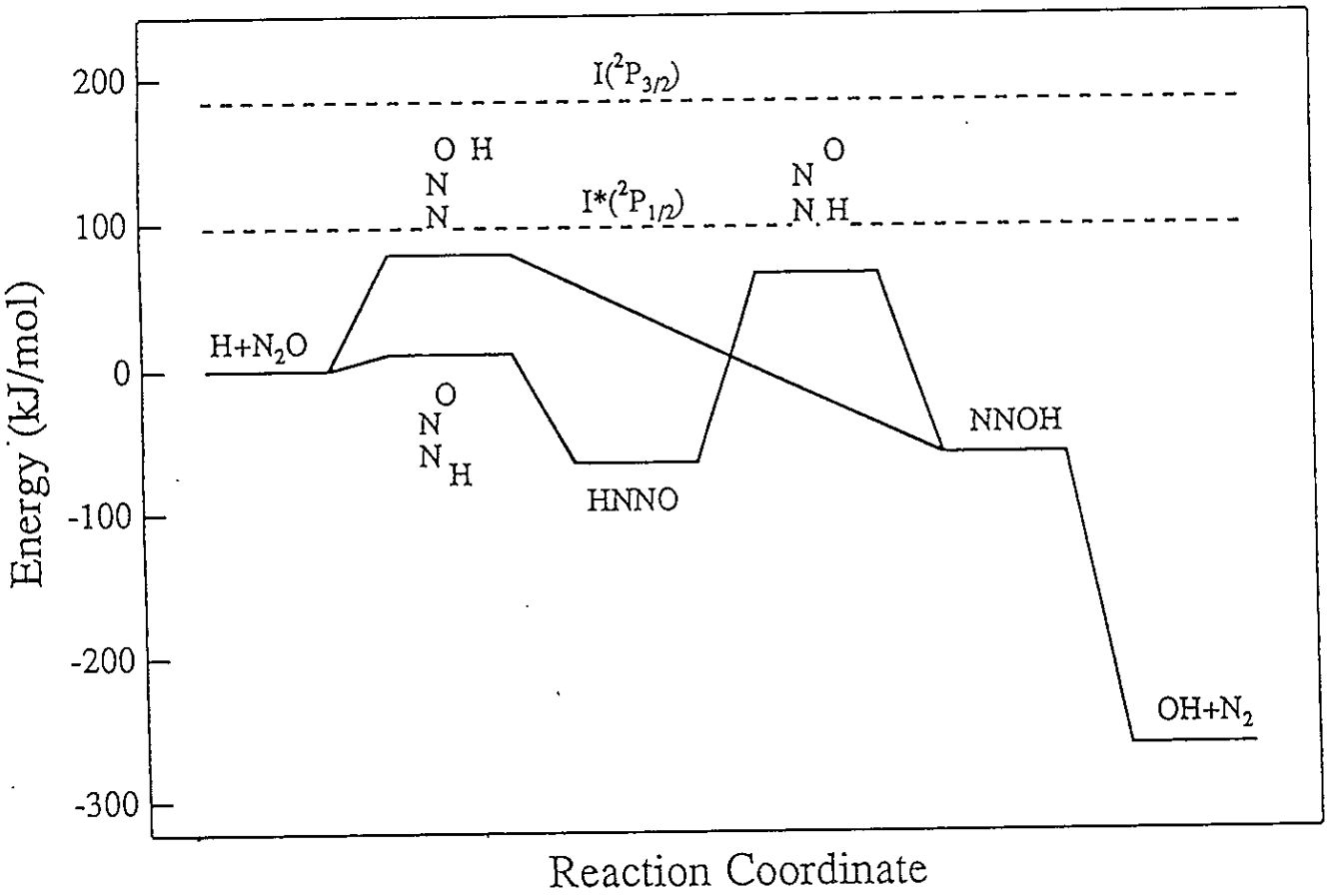

Fig.2. Potential energy diagram for the reaction $H+N_2O \rightarrow OH+N_2$. Two channels correspond to the attacks of H to the terminal N and O of N_2O.

Type (1) Conformer (calculated)

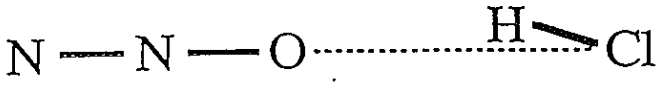

Type (2) Conformer (calculated and observed)

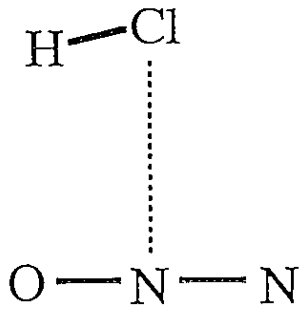

Type (3) Conformer (calculated)

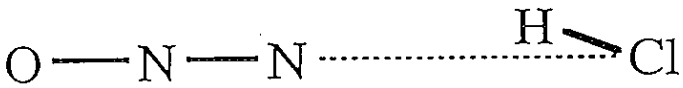

Fig. 3. Structures of three stable conformers of $HCl \cdot N_2O$ complex.

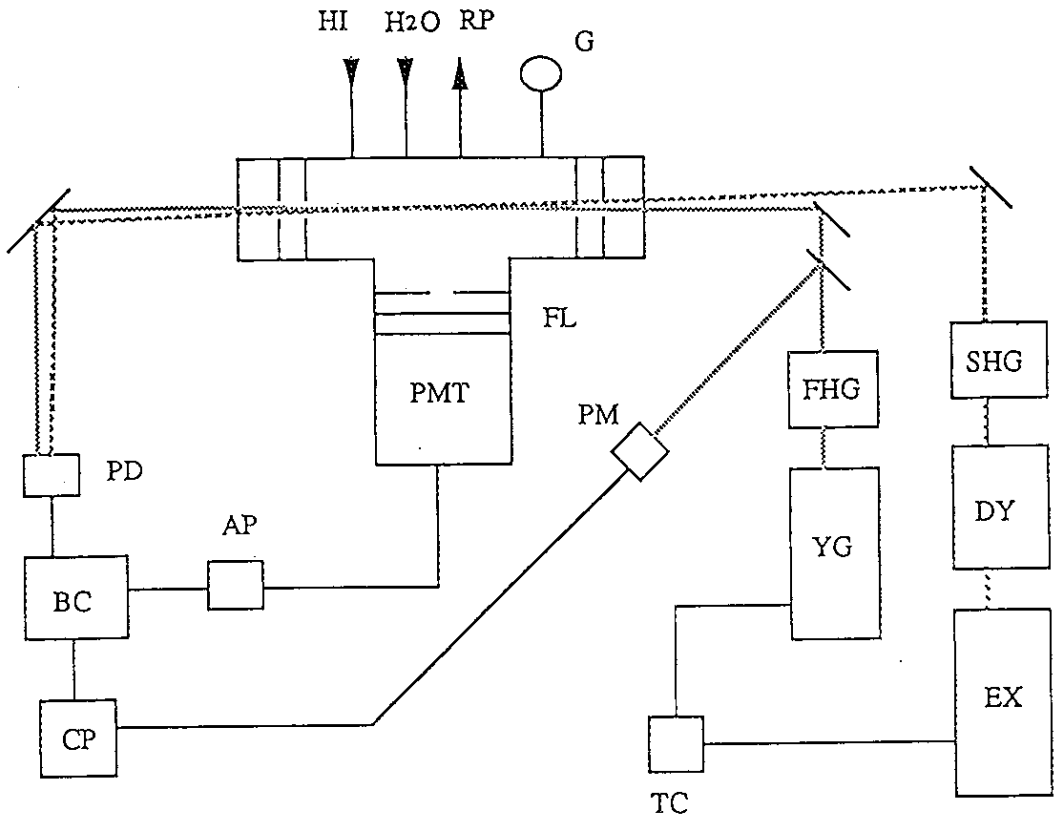

Fig. 4. Experimental setup for the bulk experiment.
(YG: Nd:YAG laser, EX: Excimer laser, DY: dye laser, SHG: second harmonic generator, FHG: fourth harmonic generator, TC: timing circuit, G: capacitance manometer, RP: rotary pump, PMT: photo-multiplier, FL: filter, PD: photodiode, PM: power meter, AP: amplifier, BC: boxcar, CP: computer)

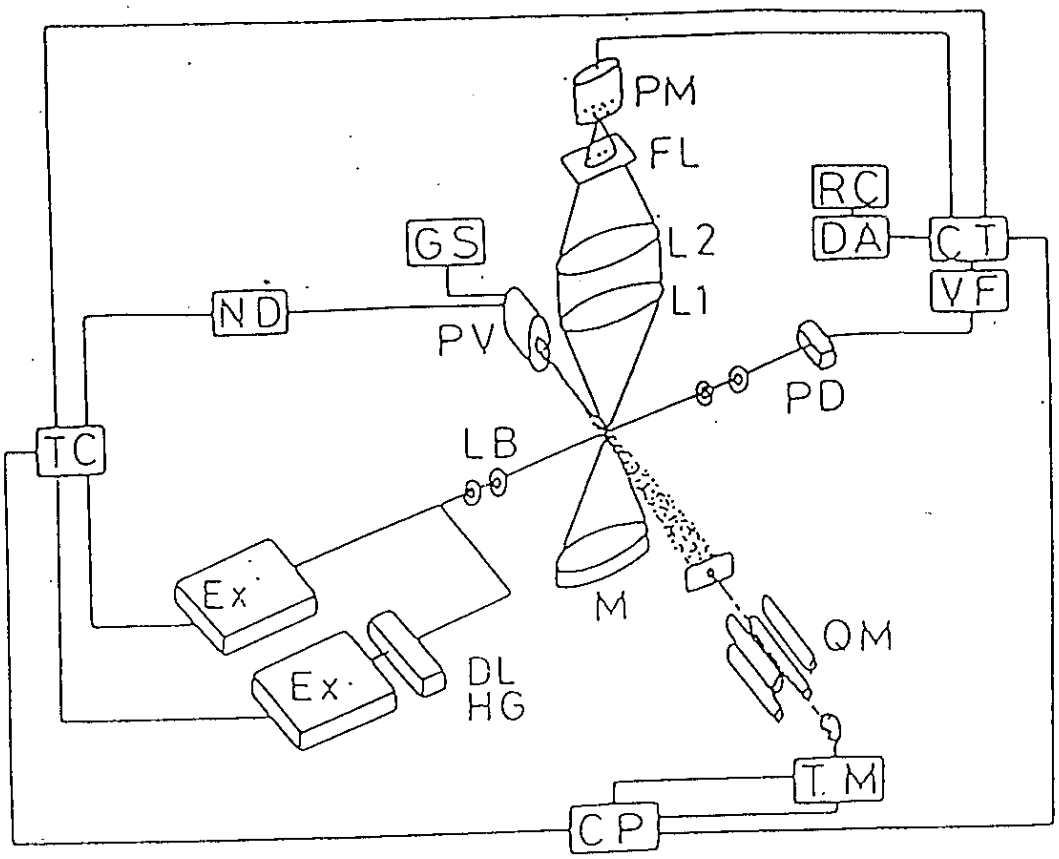

Fig. 5. Experimental setup for the free jet experiment.
(PV: pulsed valve, Ex: excimer laser, DL: dye laser, HG: harmonic generator, LB: light buffle, M: concave mirror, L1, L2: lense, FL: filter, PM: photomultiplier, PD: photodiode, VF: V-F converter, CT: counter, DA: D-A converter, RC: recorder, QM: quadrupole mass filter, TM: transient memory, CP: computer, TC: timing circuit, ND: nozzle driver, GS: gas handling system)

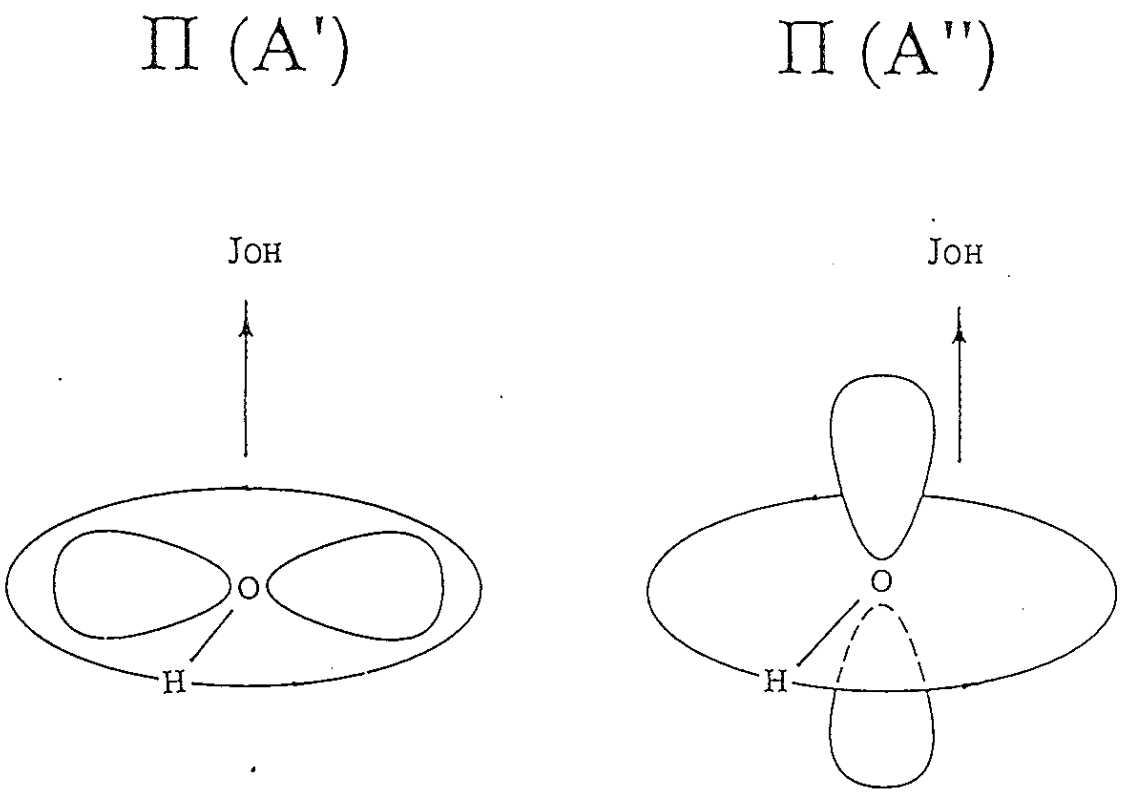

Fig. 6. The Λ-doublet components of a Π molecule (OH) in the high J limit.

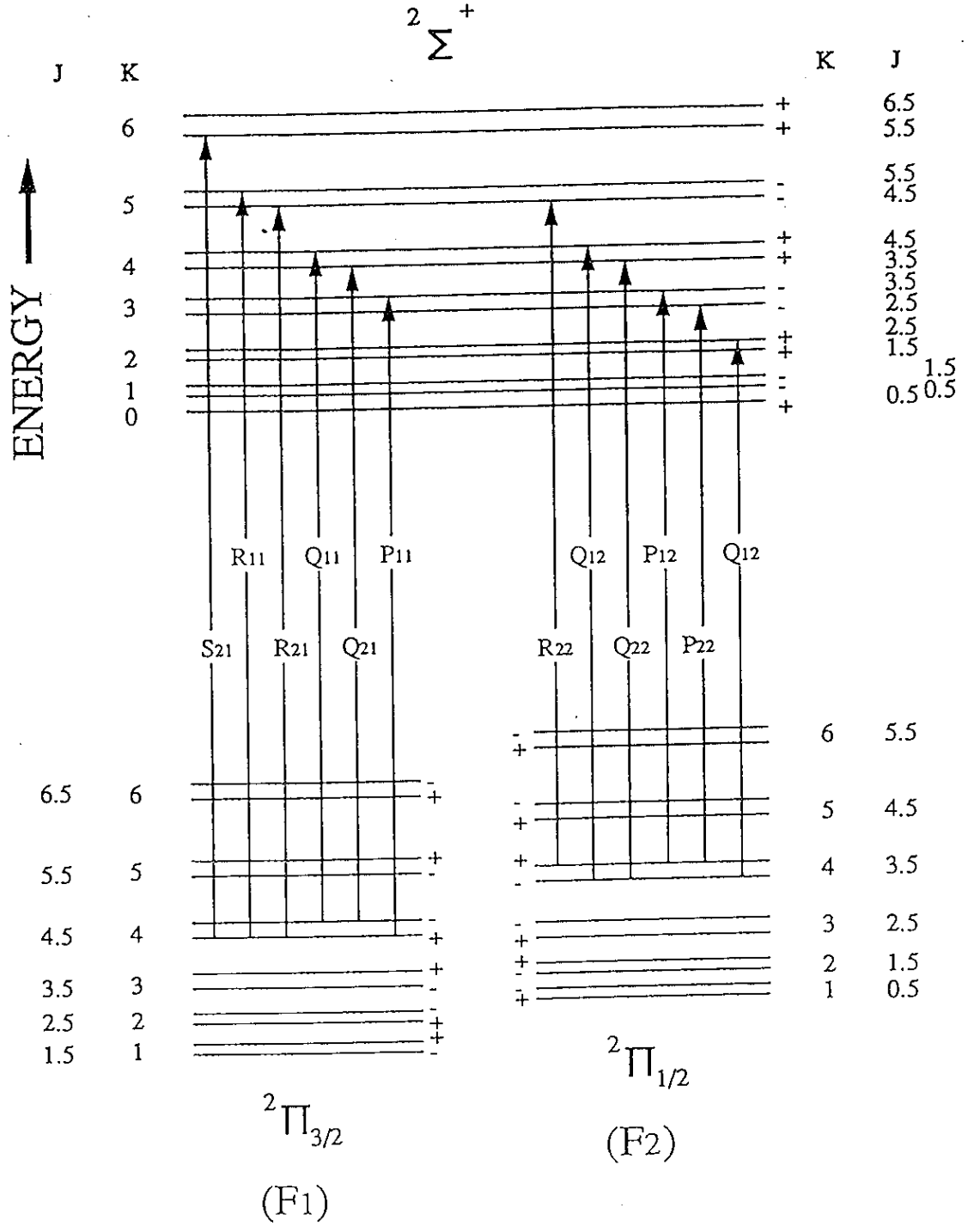

Fig. 7. Energy level diagram of OH radical.

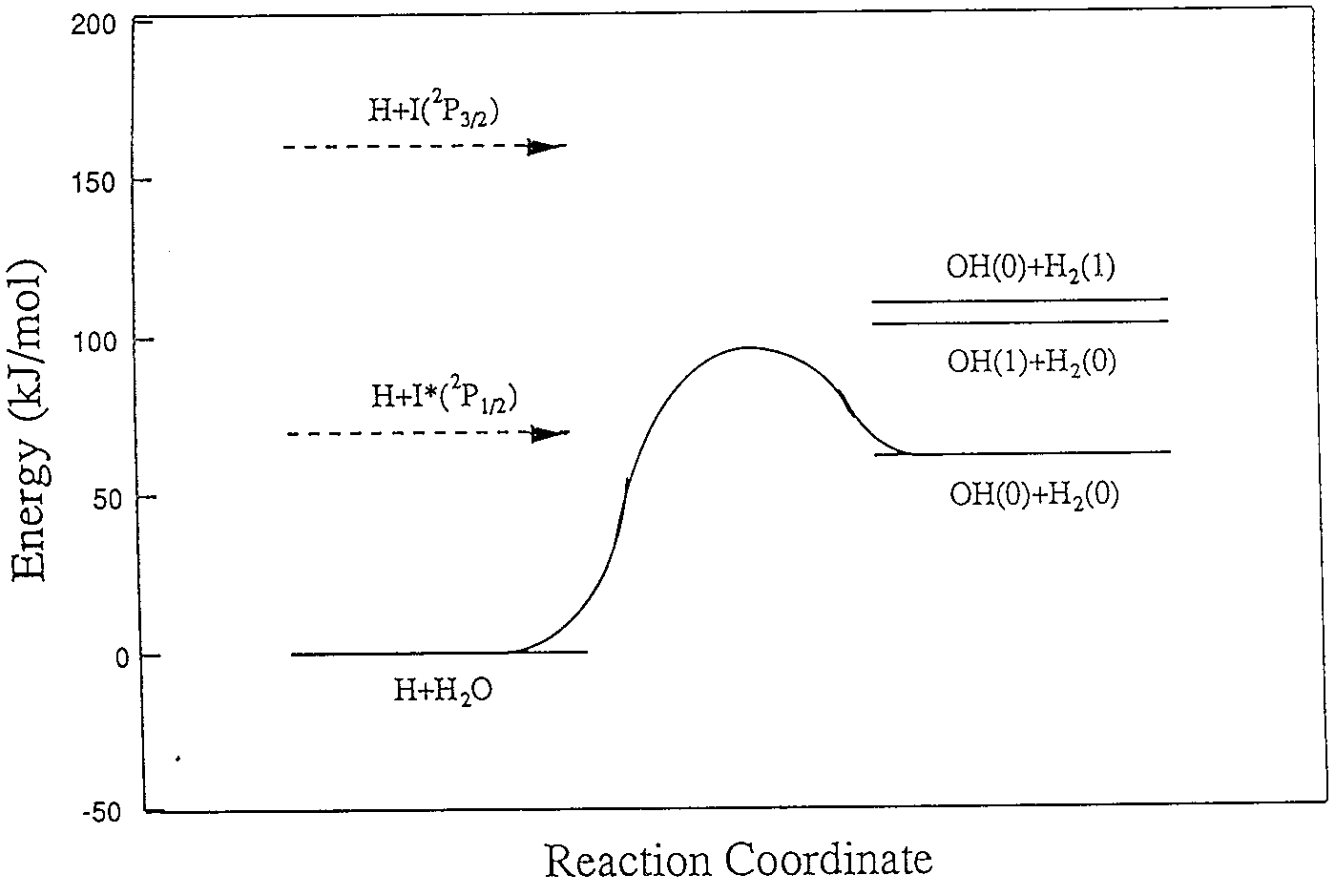

Fig. 8. Potential energy diagram for the reaction $H+H_2O \rightarrow OH+H_2$.

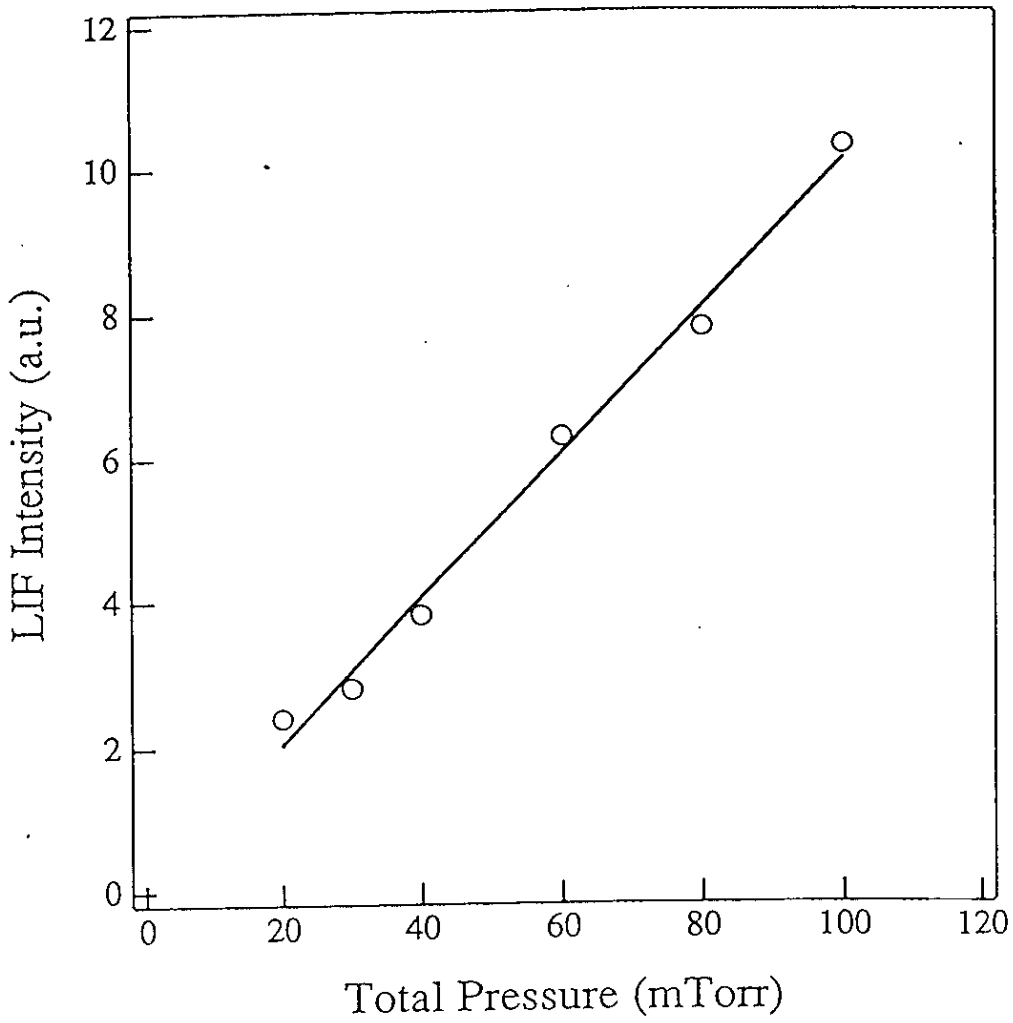

Fig. 9. Total gas pressure dependence of the LIF intensity of OH ($X^2\Pi_{3/2}$,v"=0) for the reaction $H+H_2O$ under the bulk condition. $HI:H_2O$=1:1. The data shown is for K=5.

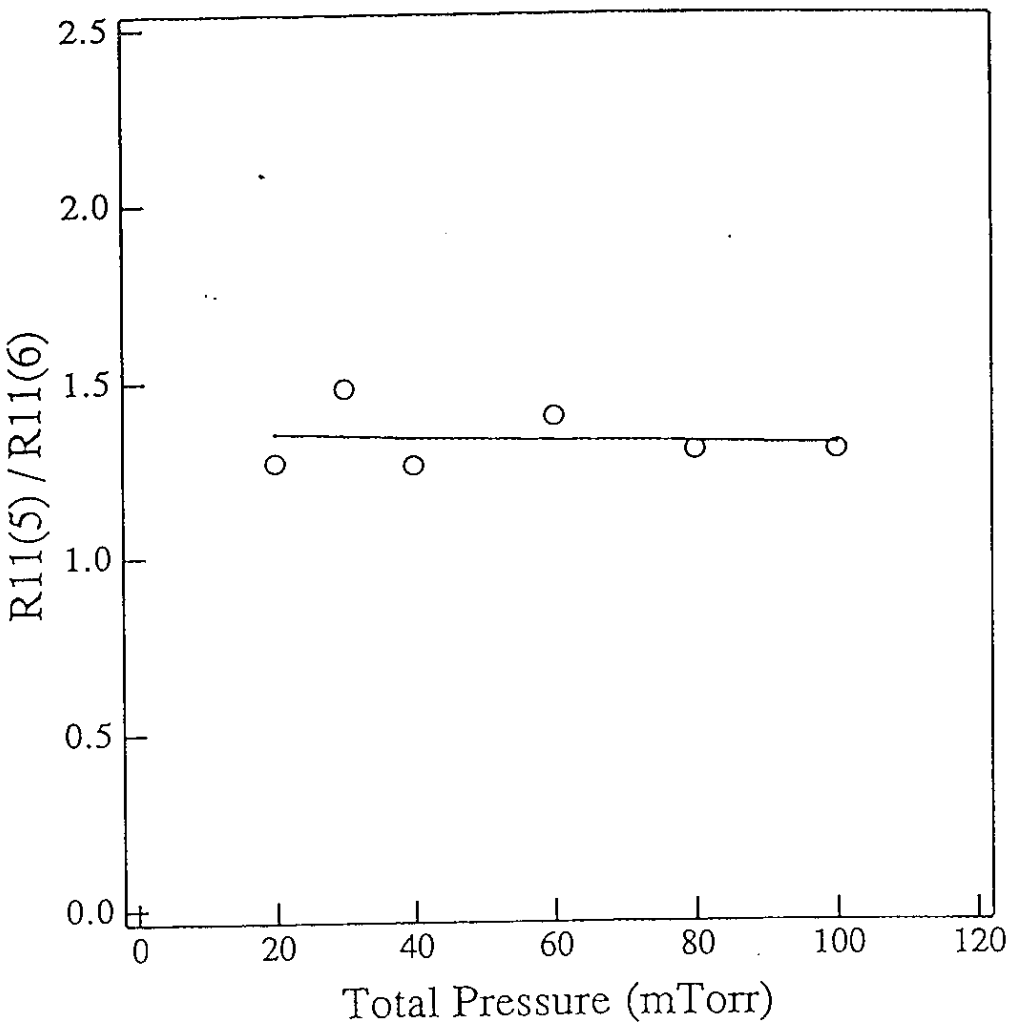

Fig.10. Total gas pressure dependence of ratio of the LIF intensities of OH ($X^2\Pi_{3/2}$,v"=0) for the reaction H+H_2O under the bulk condition HI:H_2O=1:1.

(R_{11} (5)/R_{11}(6)).

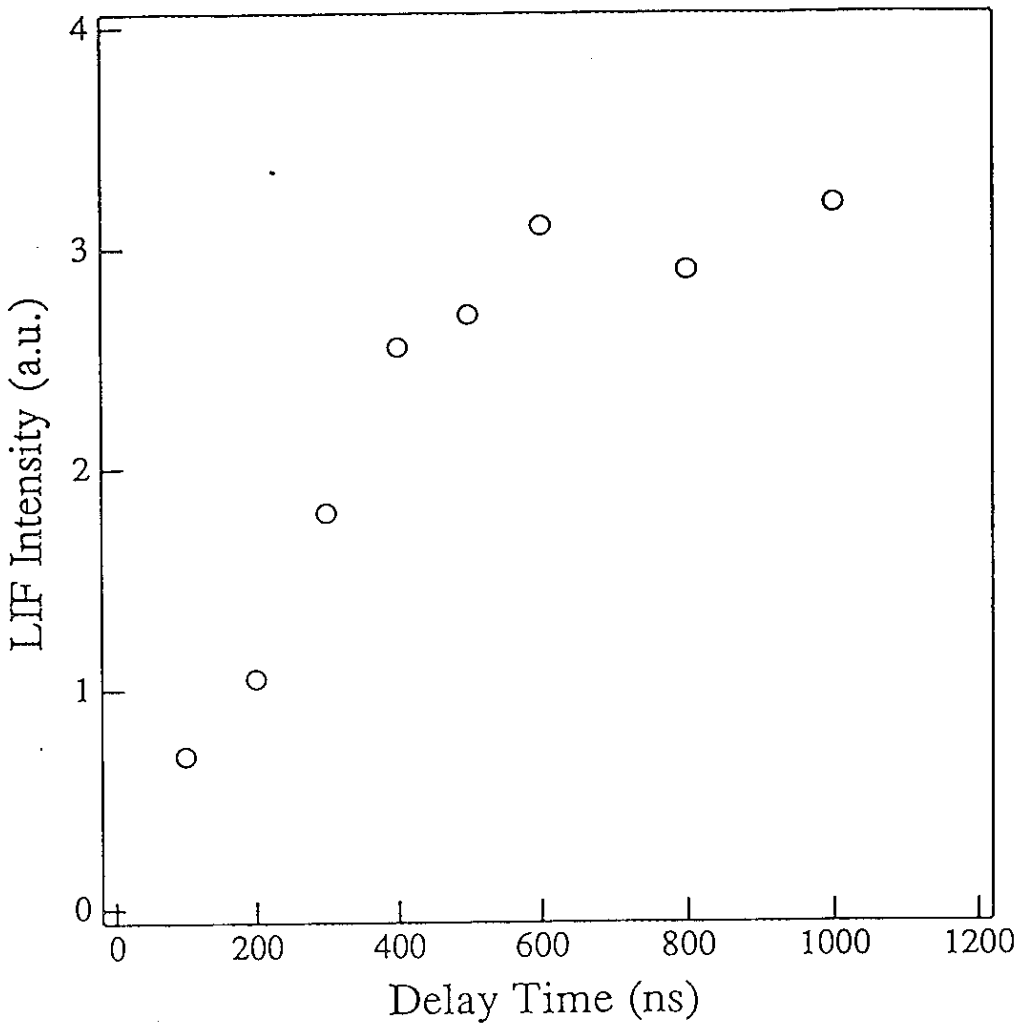

Fig.11. Pump-probe delay time dependence of the LIF intensity of OH ($X^2\Pi_{3/2}$,v"=0) for the reaction $H+H_2O$ under the bulk condition. The data shown is for K=5.

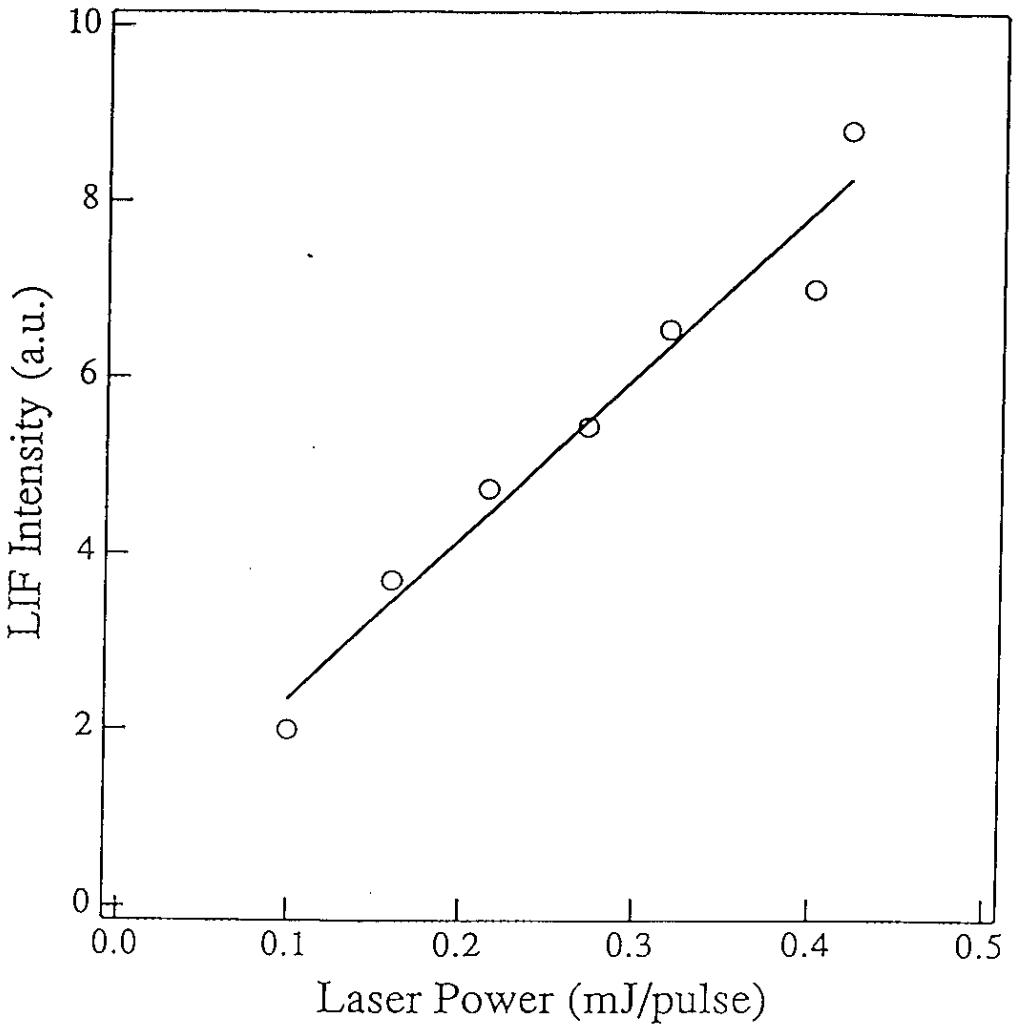

Fig.12. Laser power dependence of the LIF intensity of OH ($X^2\Pi$,v"=0) for the reaction $H+H_2O$ under the bulk condition. The data shown is for K=5.

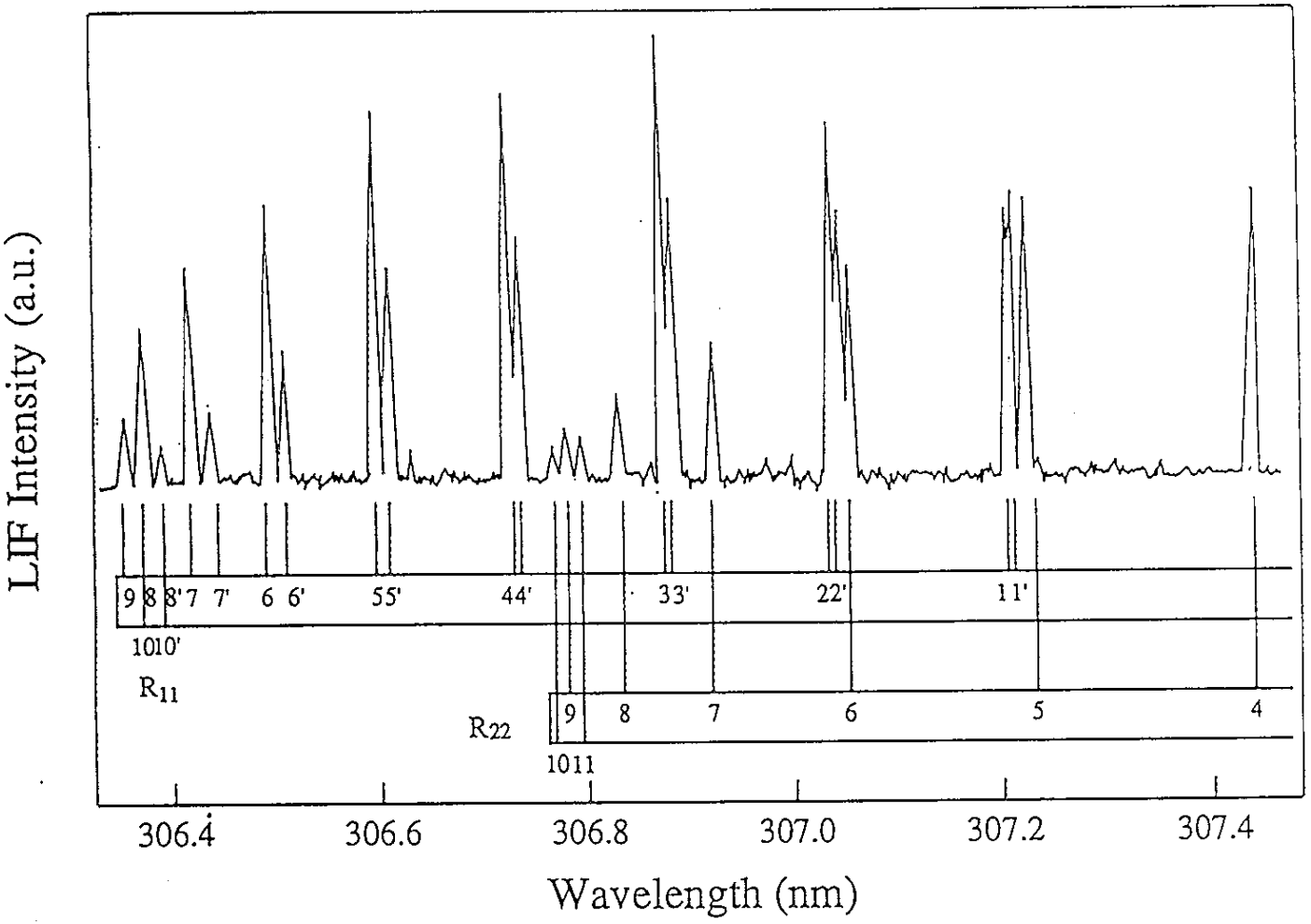

Fig.13(a). Part of the OH $A^2\Sigma^+$-$X^2\Pi$ (v"=0) LIF excitation spectrum for the reaction $H+H_2O \rightarrow OH+H_2$ under the bulk condition. (H atom is produced by the 266 nm photolysis of HI. Sample pressures of H_2O and HI are 30 mTorr. The delay time is 80 ns.)

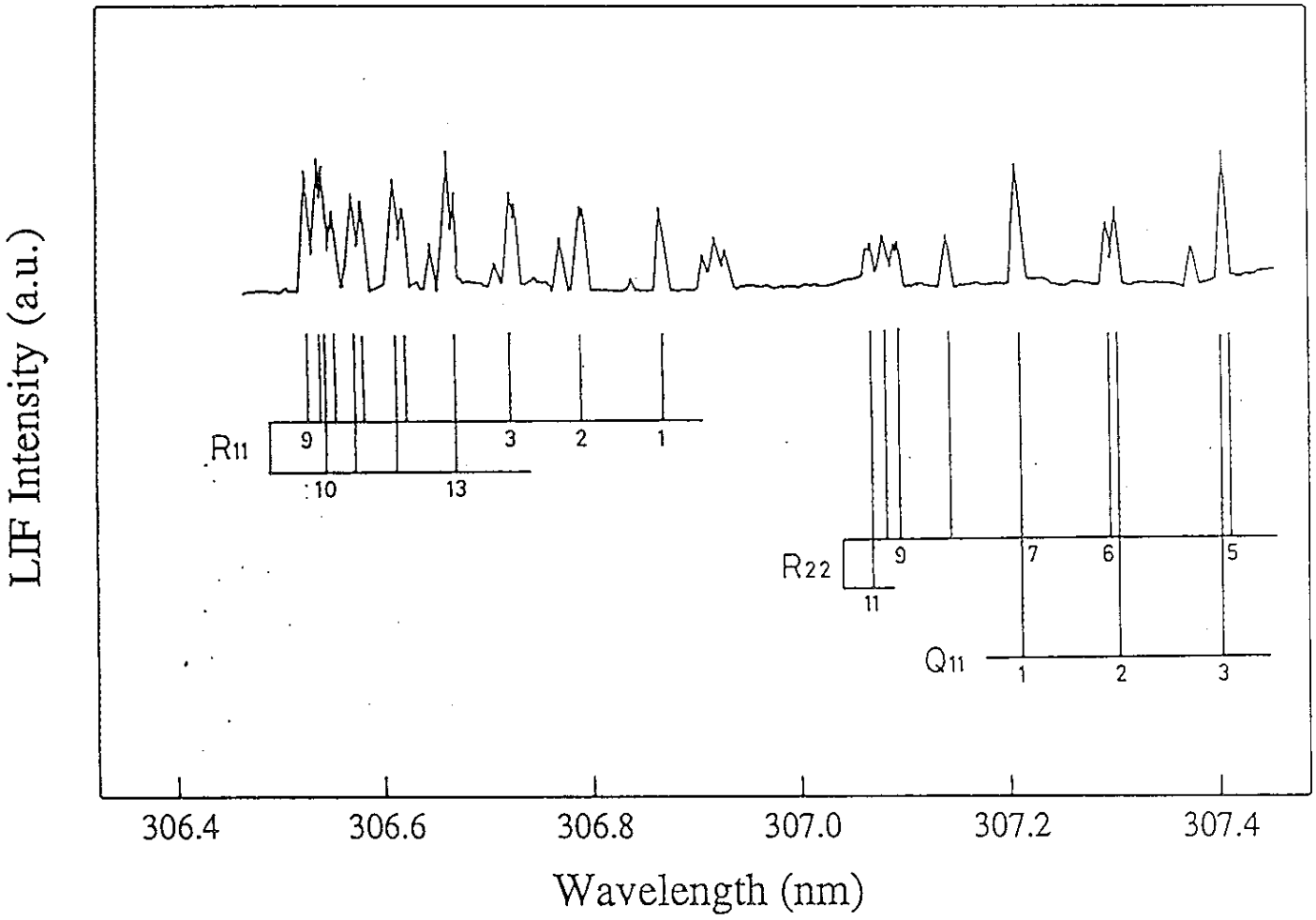

Fig.13(b). Part of the OD (v"=0) LIF excitation spectrum for the reaction $H+D_2O \rightarrow OD+HD$ under the same experimental condition as Fig.13(a).

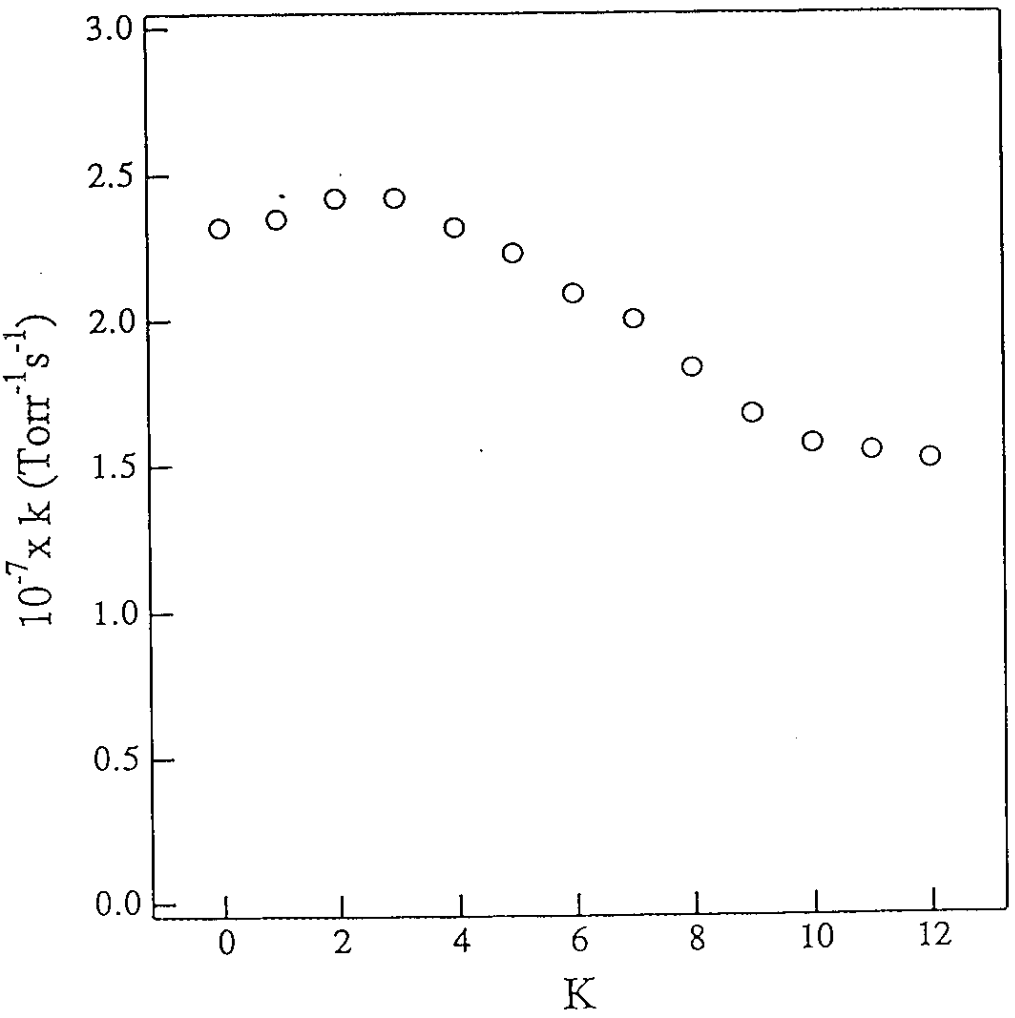

Fig.14. K dependence of OH($A^2\Sigma^+$) quenching rate constants.

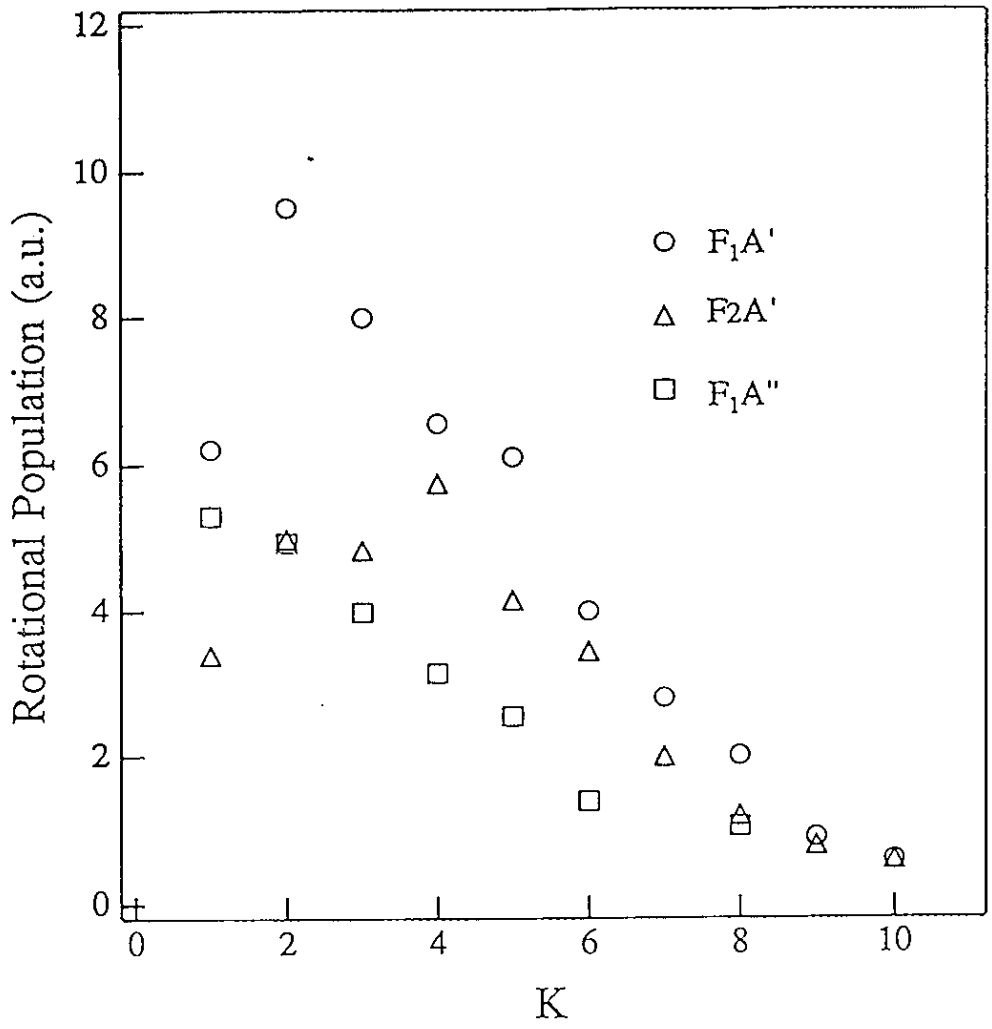

Fig.15. Nascent rotational-state distribution of OH(v"=0) for the reaction $H+H_2O$ under the bulk condition.

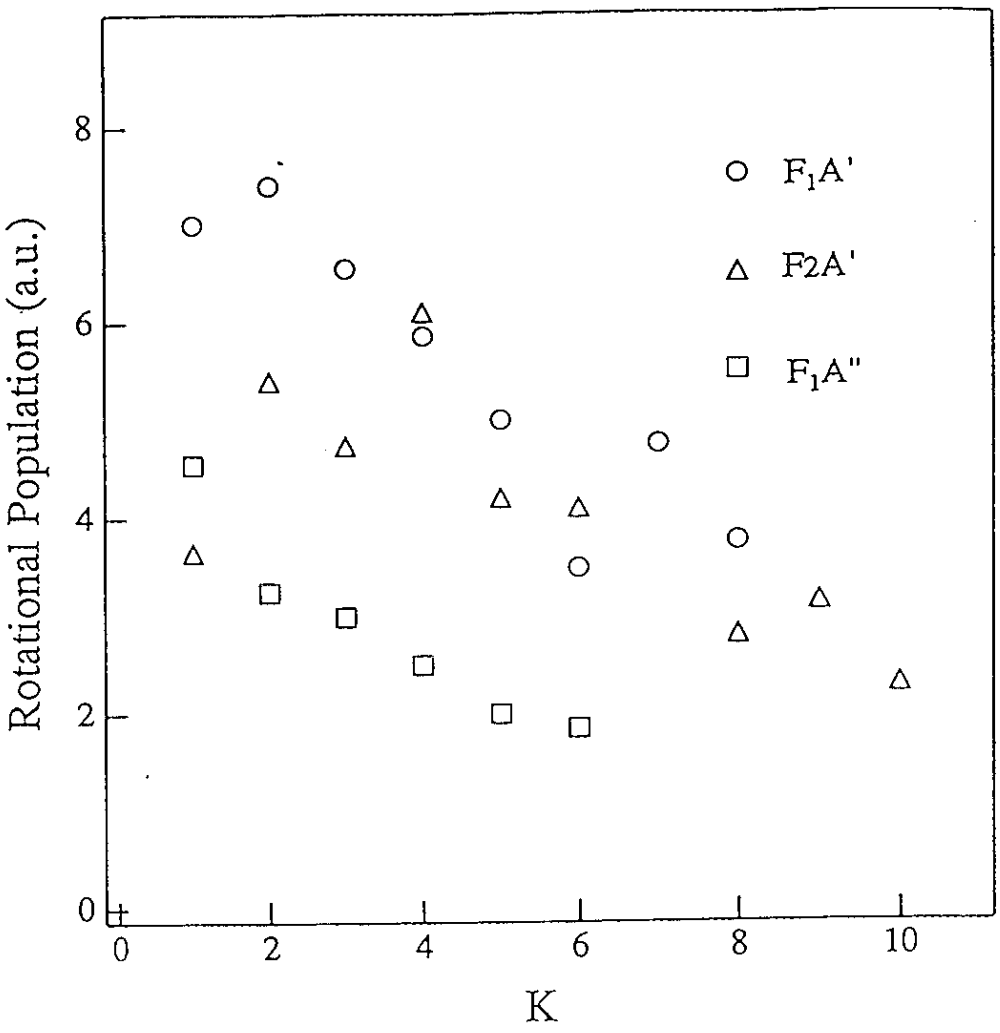

Fig.16. Nascent rotational-state distribution of OD(v"=0) for the reaction $H+D_2O$ under the bulk condition.

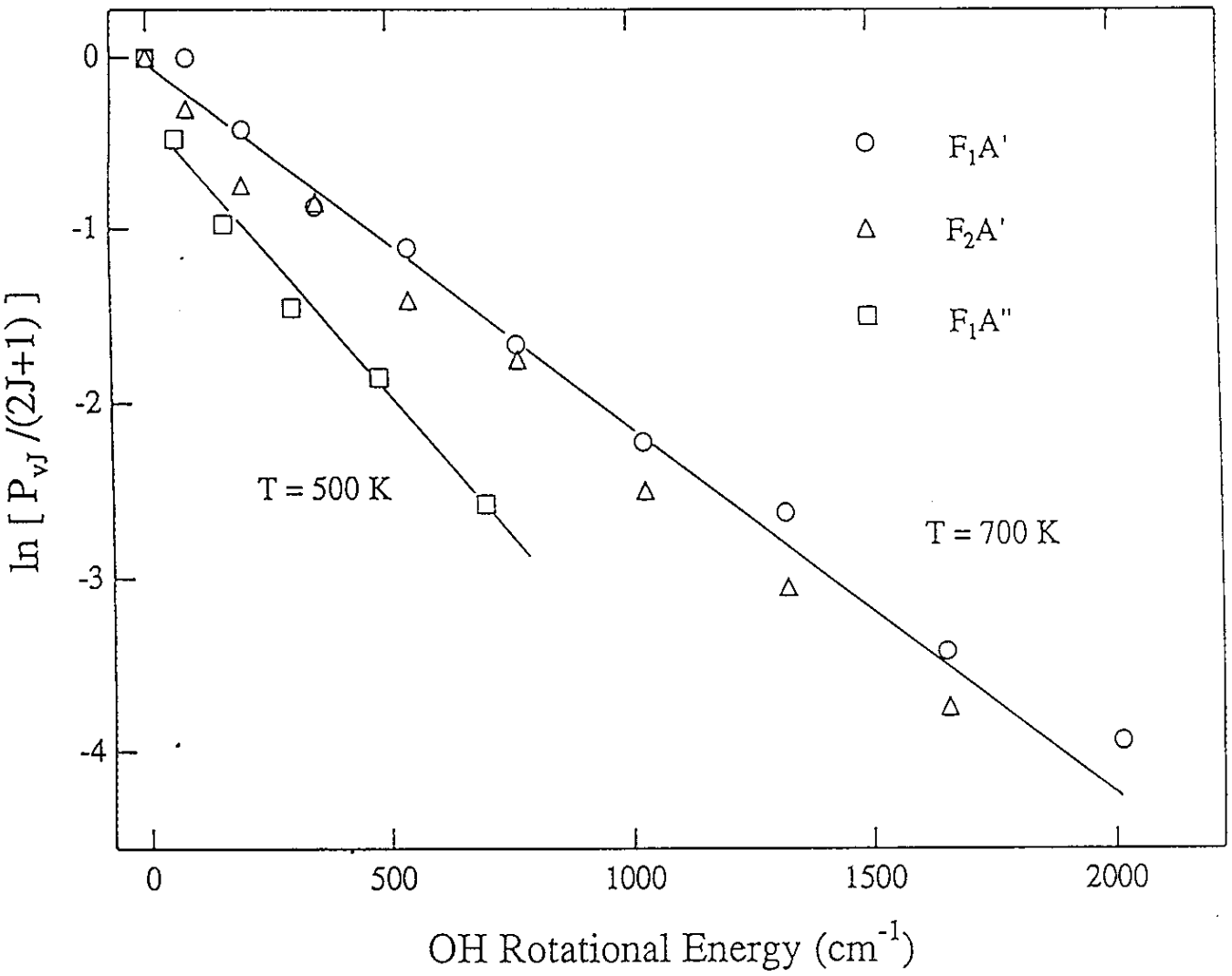

Fig.17. Boltzmann plot of the rotational distribution of OH(v"=0) for the reaction H+H_2O under the bulk condition.

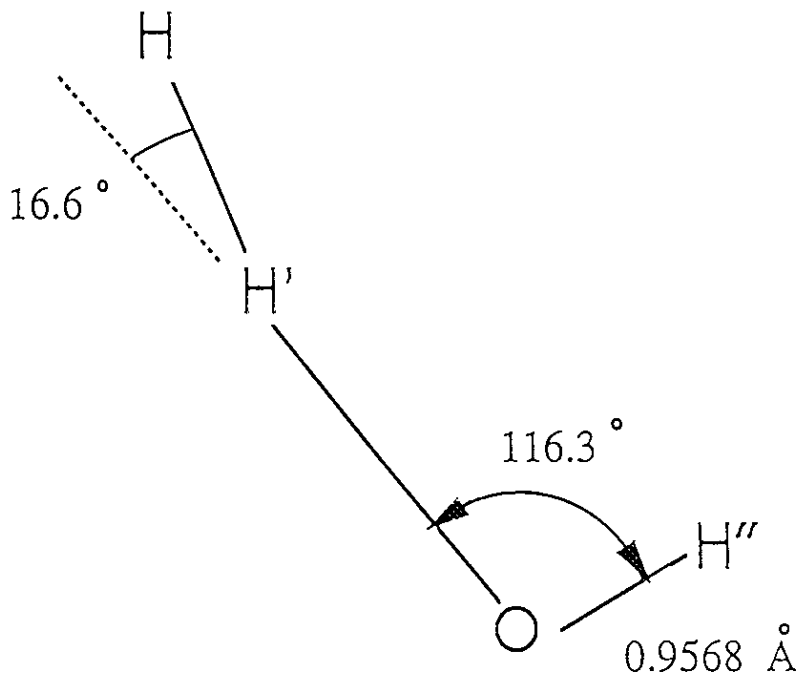

Fig.18. Transition-state geometry for the reaction $H+H_2O$.

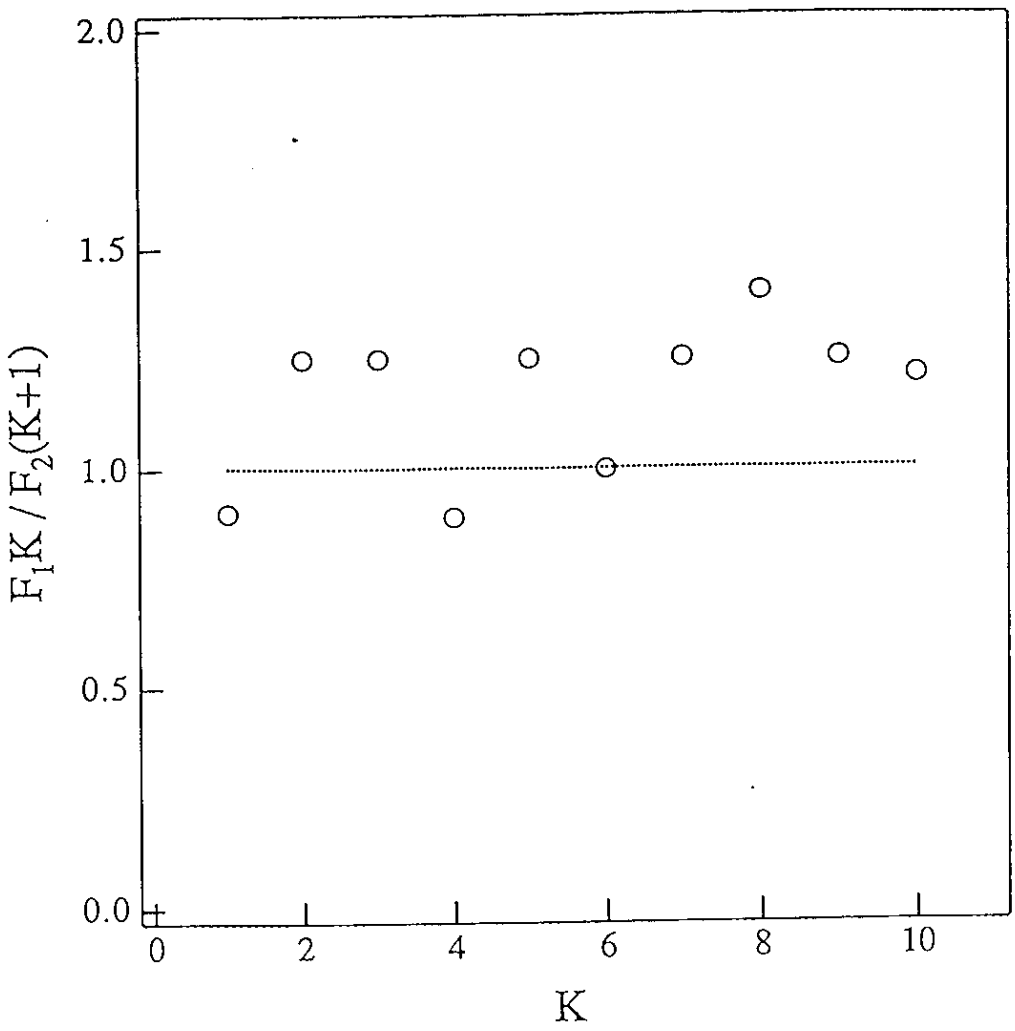

Fig.19. K dependence of spin-orbit population ratio of OH(v"=0) for the reaction $H+H_2O$ under the bulk condition.

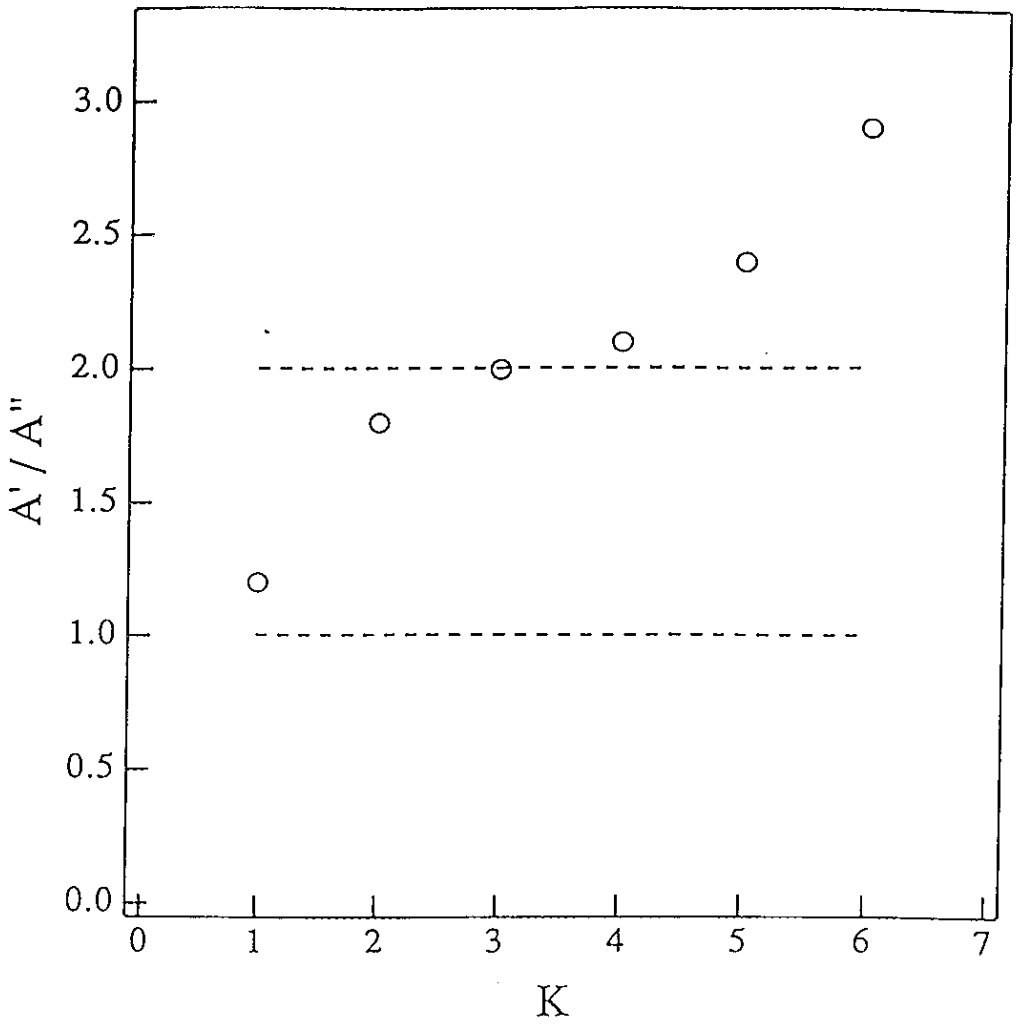

Fig.20. K dependence of Λ-doublet population ratios of OH(v"=0) for the reaction H+H_2O under the bulk condition.

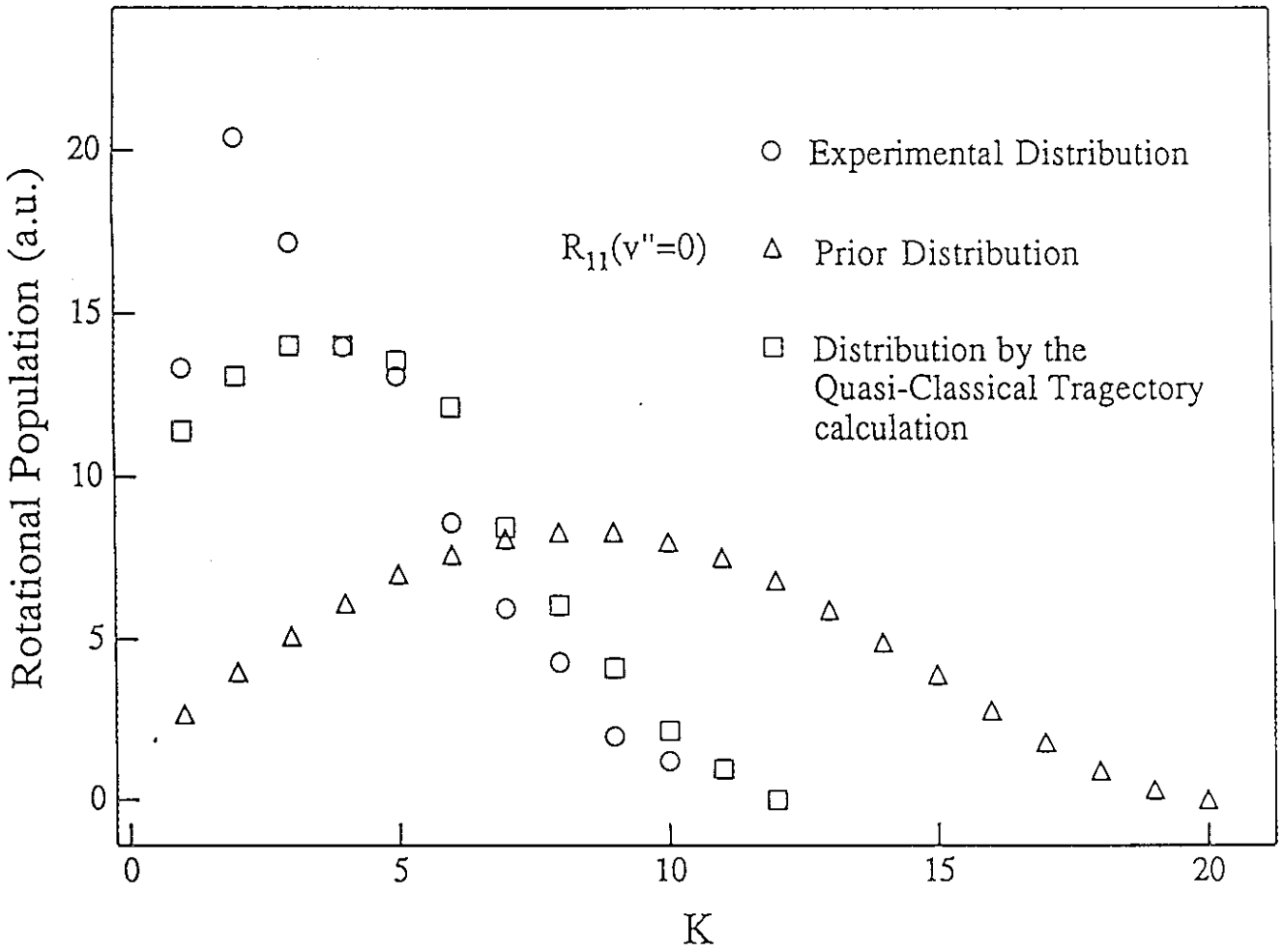

Fig.21(a). Comparison between experimental and calculated distributions of OH(v"=0) rotational states for the reaction H+H_2O under the bulk condition.

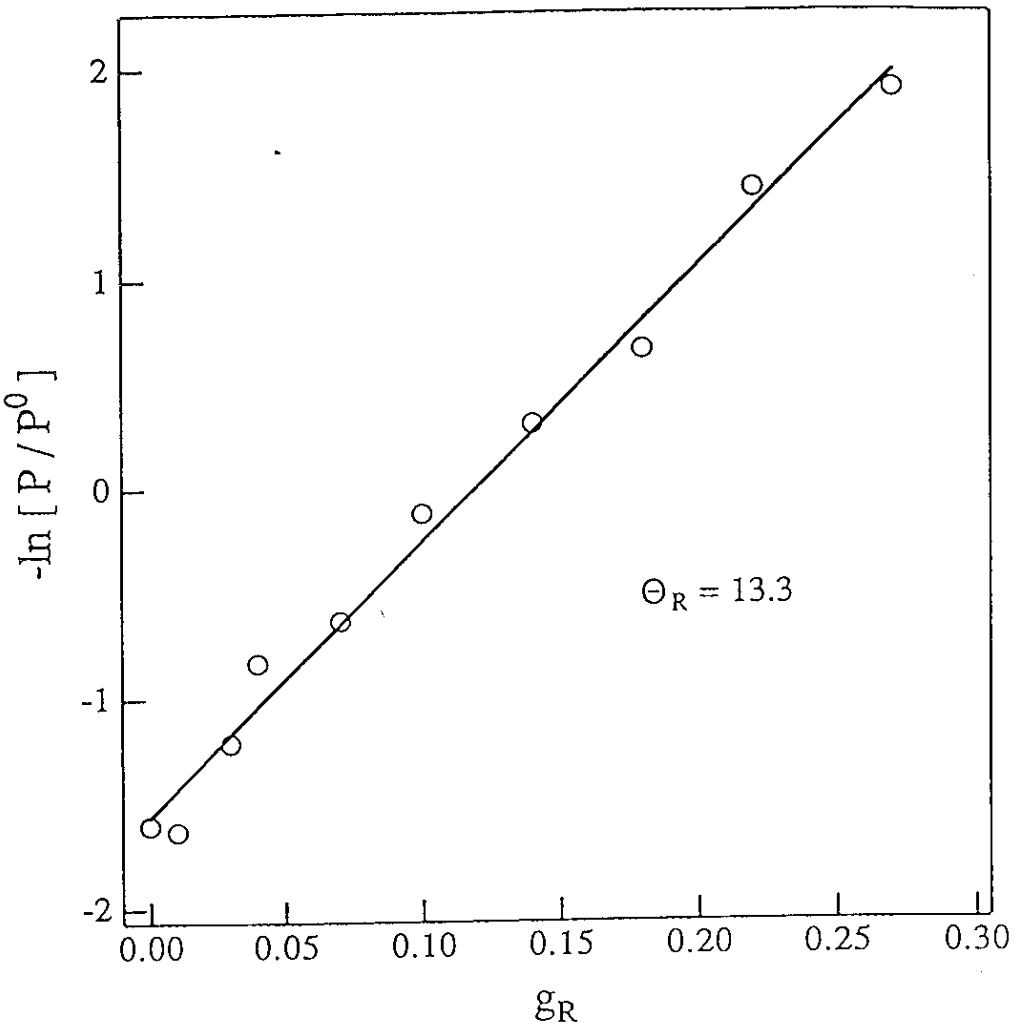

Fig.21(b). Suprisal plot of rotational distribution of OH(v"=0) for the reaction H+H_2O under the bulk condition.

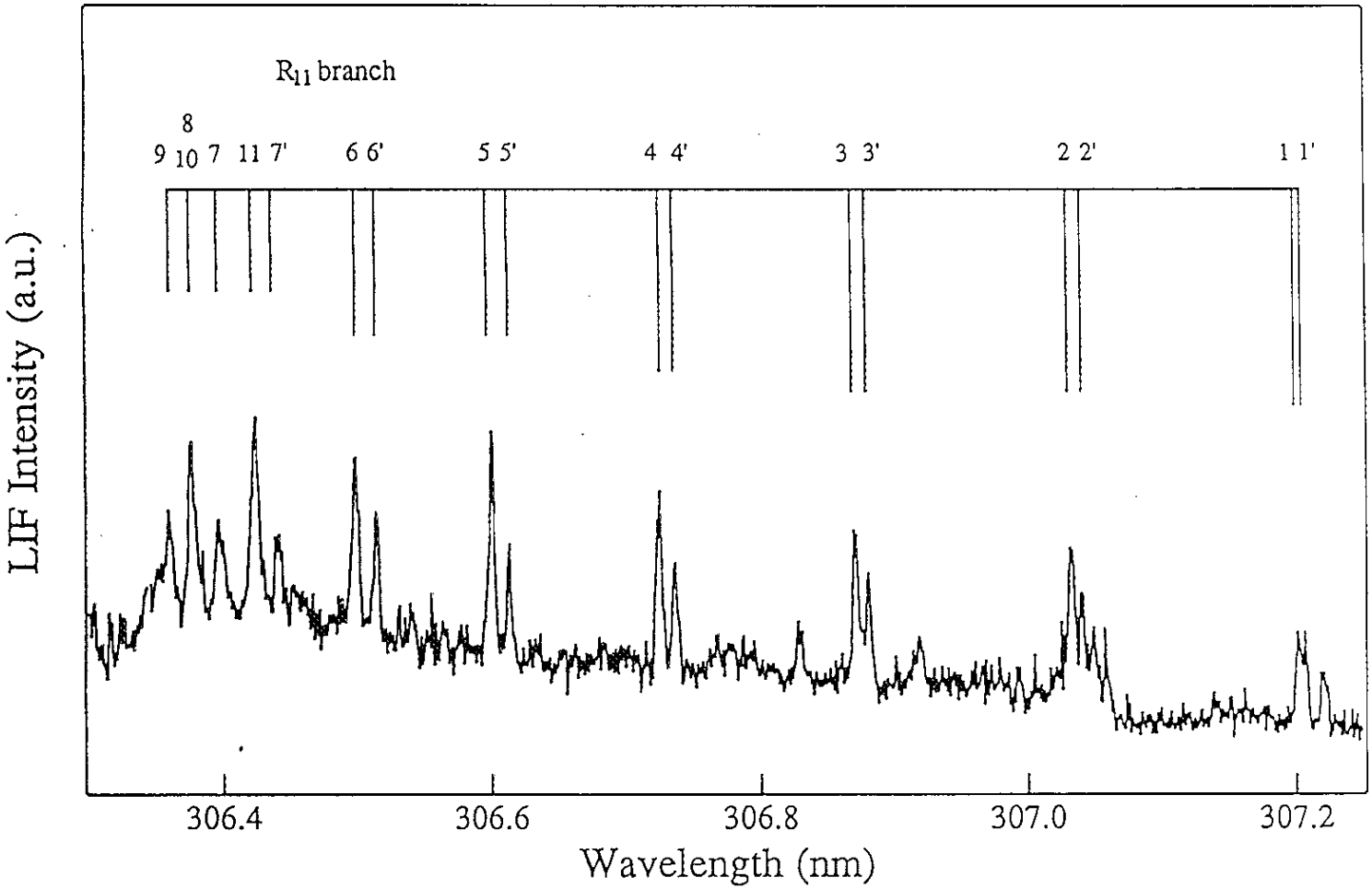

Fig.22. OH $A^2\Sigma^+$ (v"=0) LIF excitation spectrum for the reaction $HBr{\cdot}H_2O \rightarrow OH+H_2+Br$ under the reactant-pair condition.
(Stagnation pressure is 2.0 atm. Pump-probe delay time is 200 ns.
$HBr:H_2O:He$ = 2.6:0.9:96.5.)

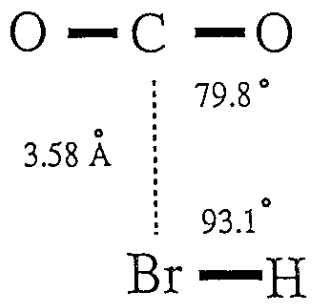

(a) Type (1) Conformer
(observed and calculated)

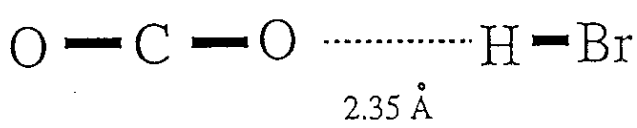

(b) Type (2) Conformer
(calculated)

Fig.23. Structures of two stable conformers of $HBr \cdot CO_2$ complex.

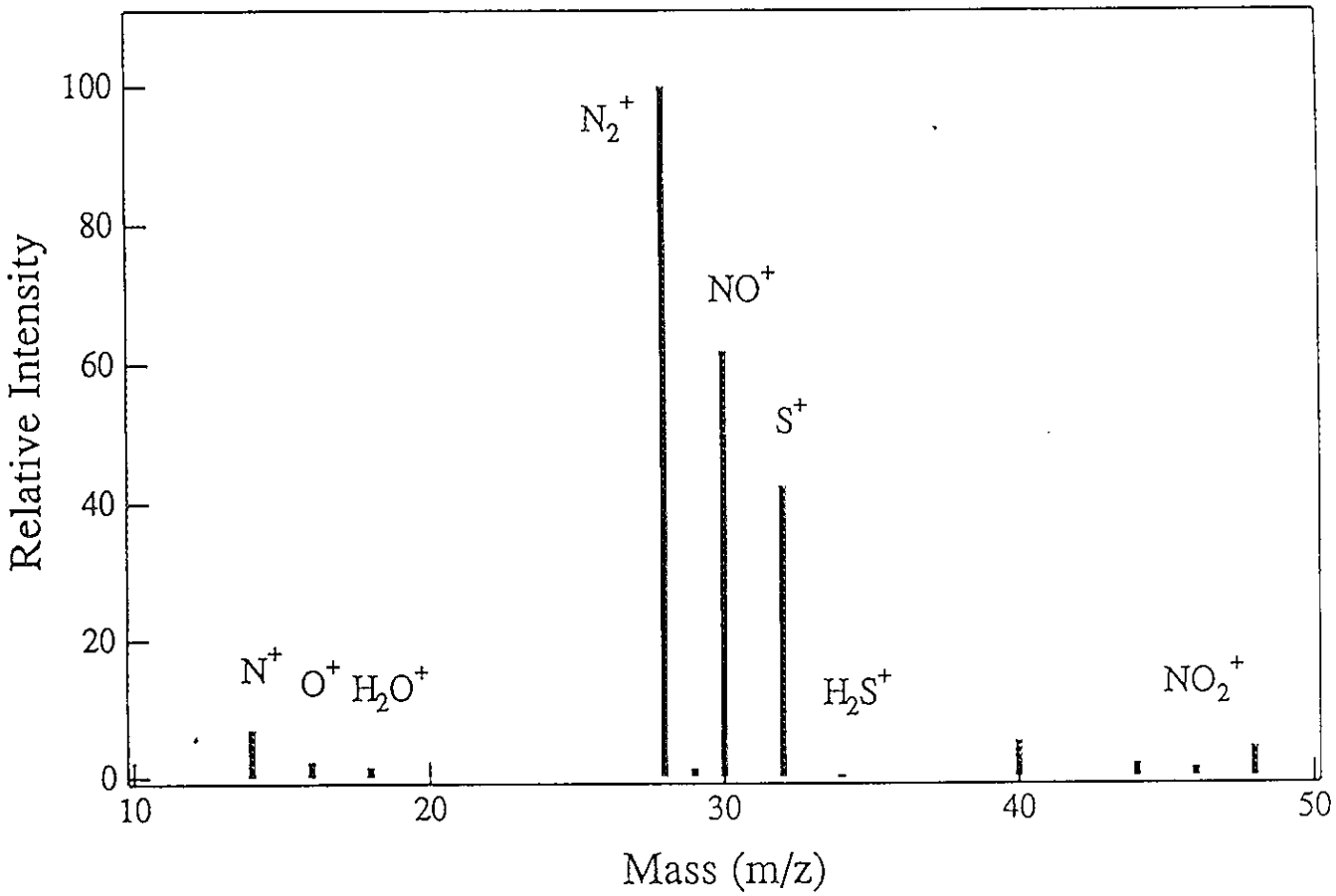

Fig.24. Mass spectrum of gas mixture of NO_2 and H_2S.

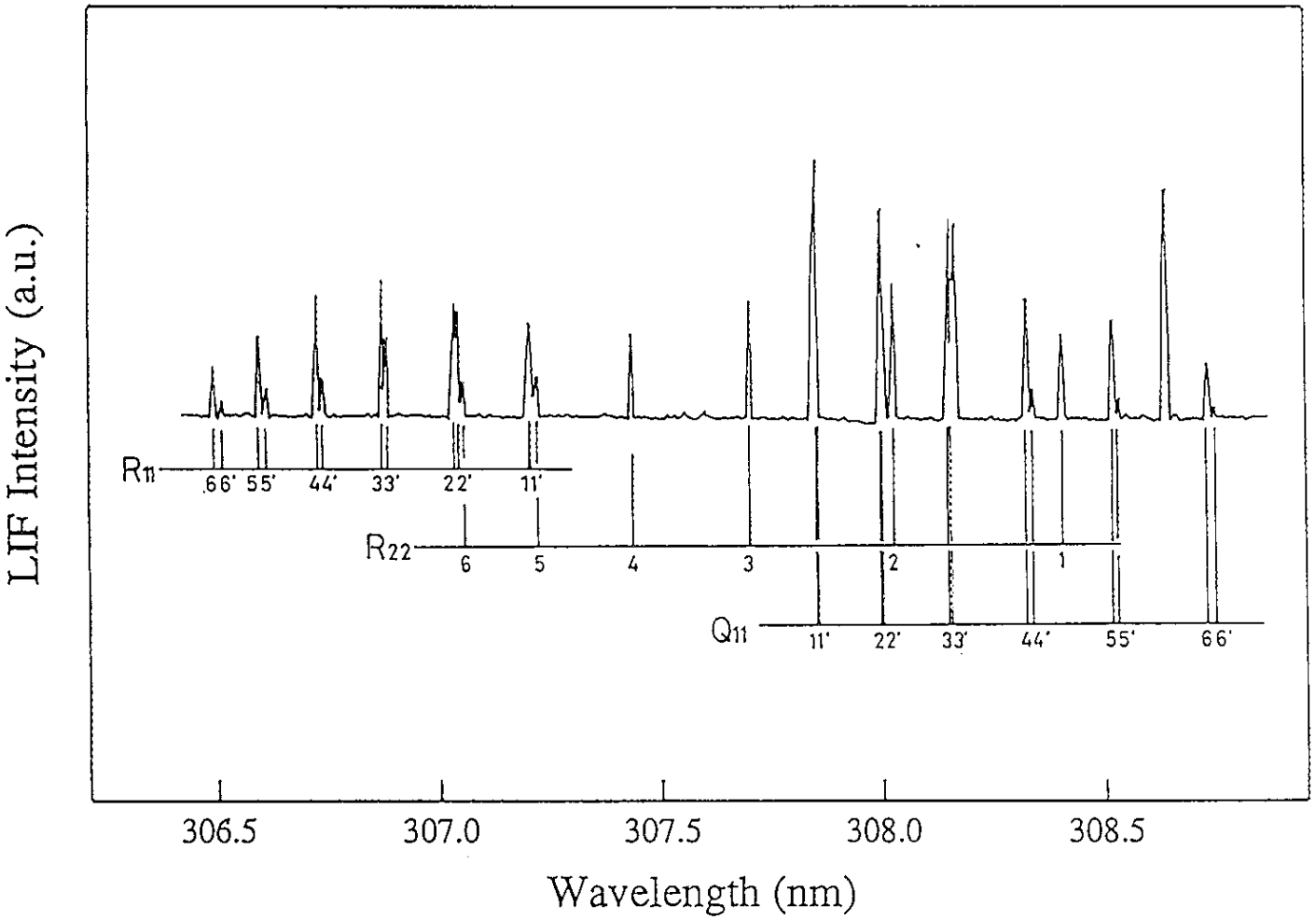

Fig.25. Part of the OH $A^2\Sigma^+$-$X^2\Pi$ (v"=0) LIF excitation spectrum for $O(^3P)+H_2S \rightarrow OH+HS$ under the bulk condition.
(H atom is produced by the 355 nm photolysis of NO_2. Sample pressures of H_2S and NO_2 are 5 mTorr. The delay time is 200 ns.)

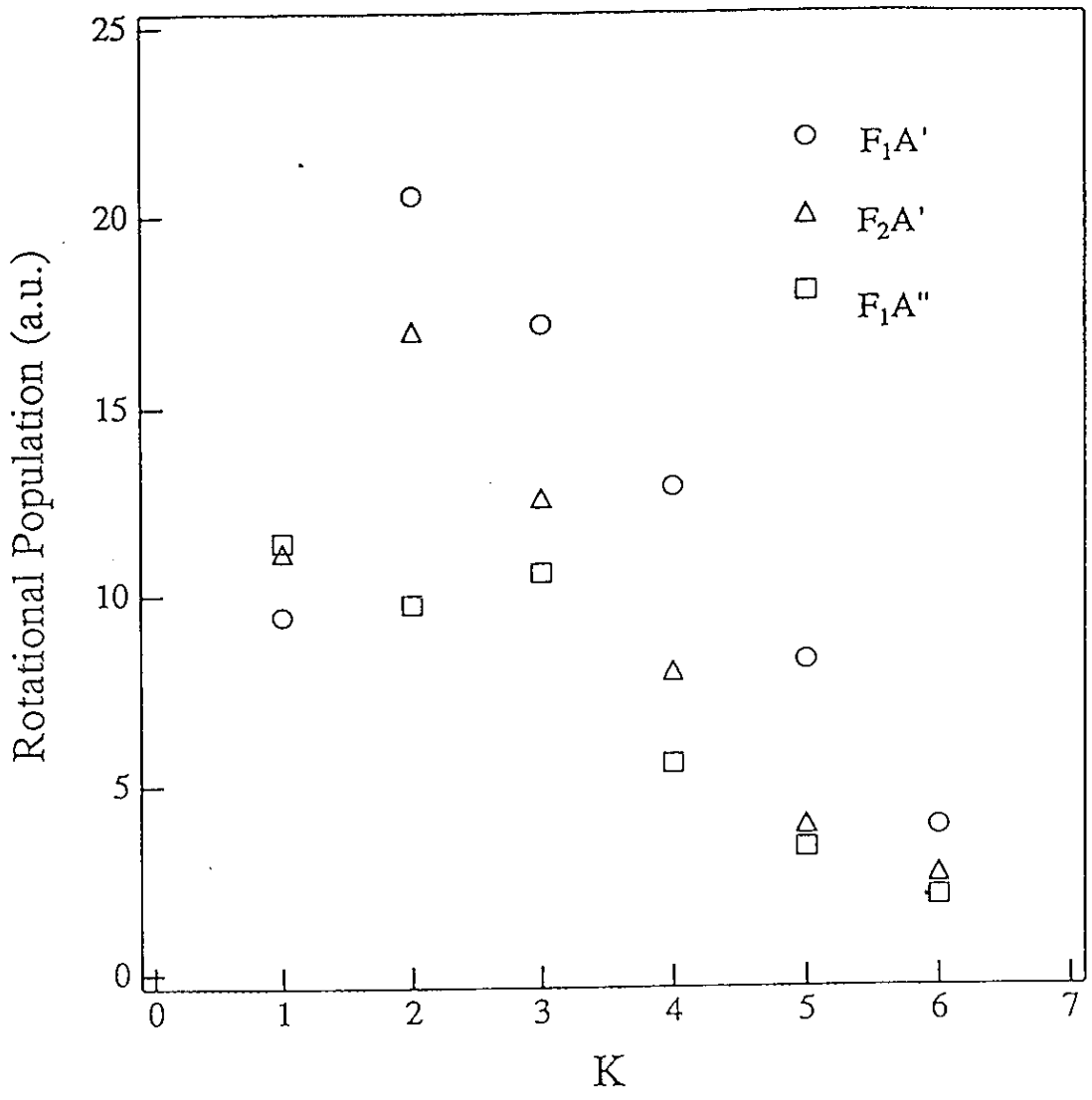

Fig.26. Nascent rotational state distribution of OH (v"=0) for the reaction $O(^3P)+H_2S$ under the bulk condition.

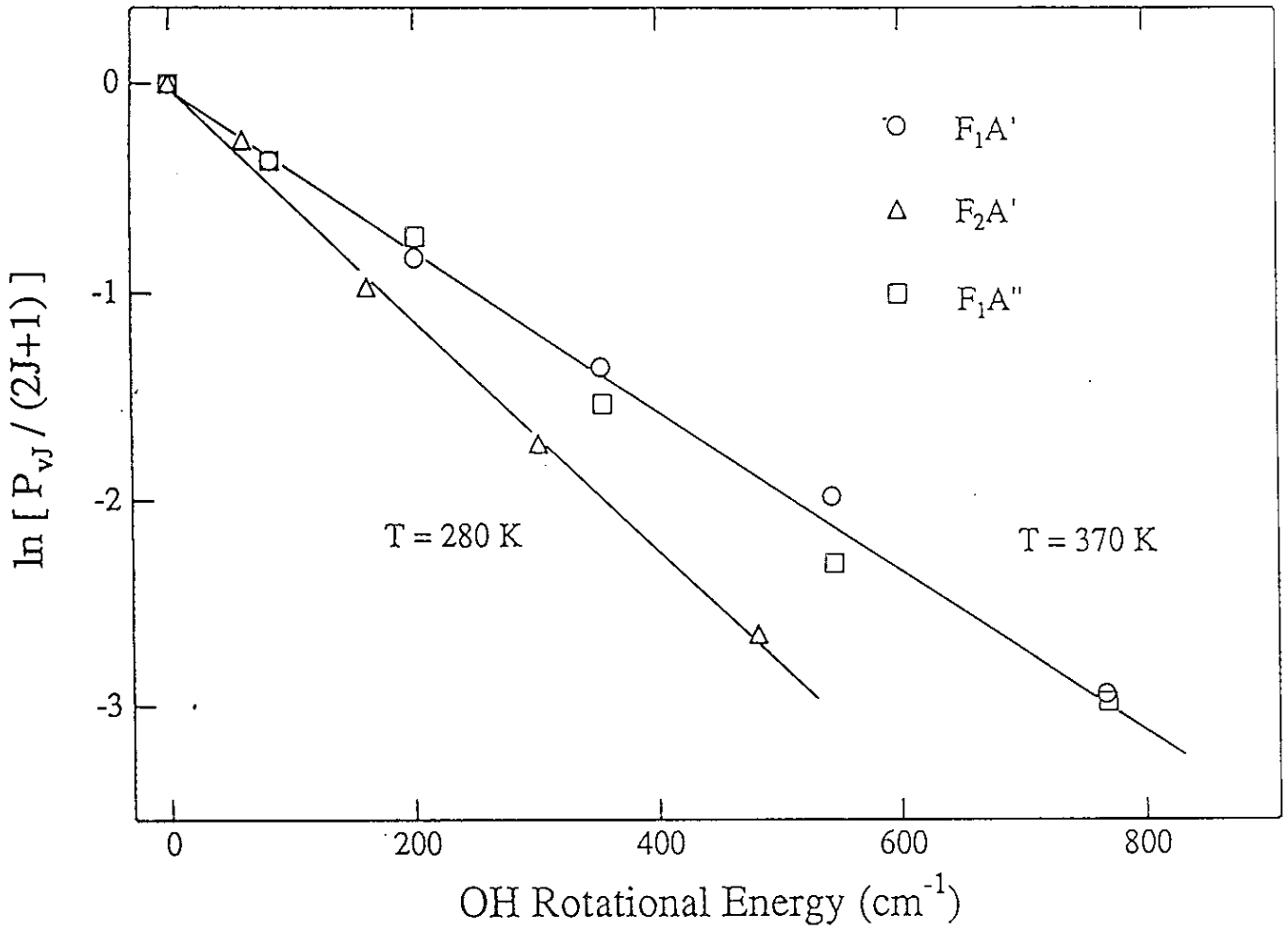

Fig.27. Boltzmann plot of the rotational distribution of OH(v"=0) for the $O(^3P)+H_2S$ reaction under the bulk condition.

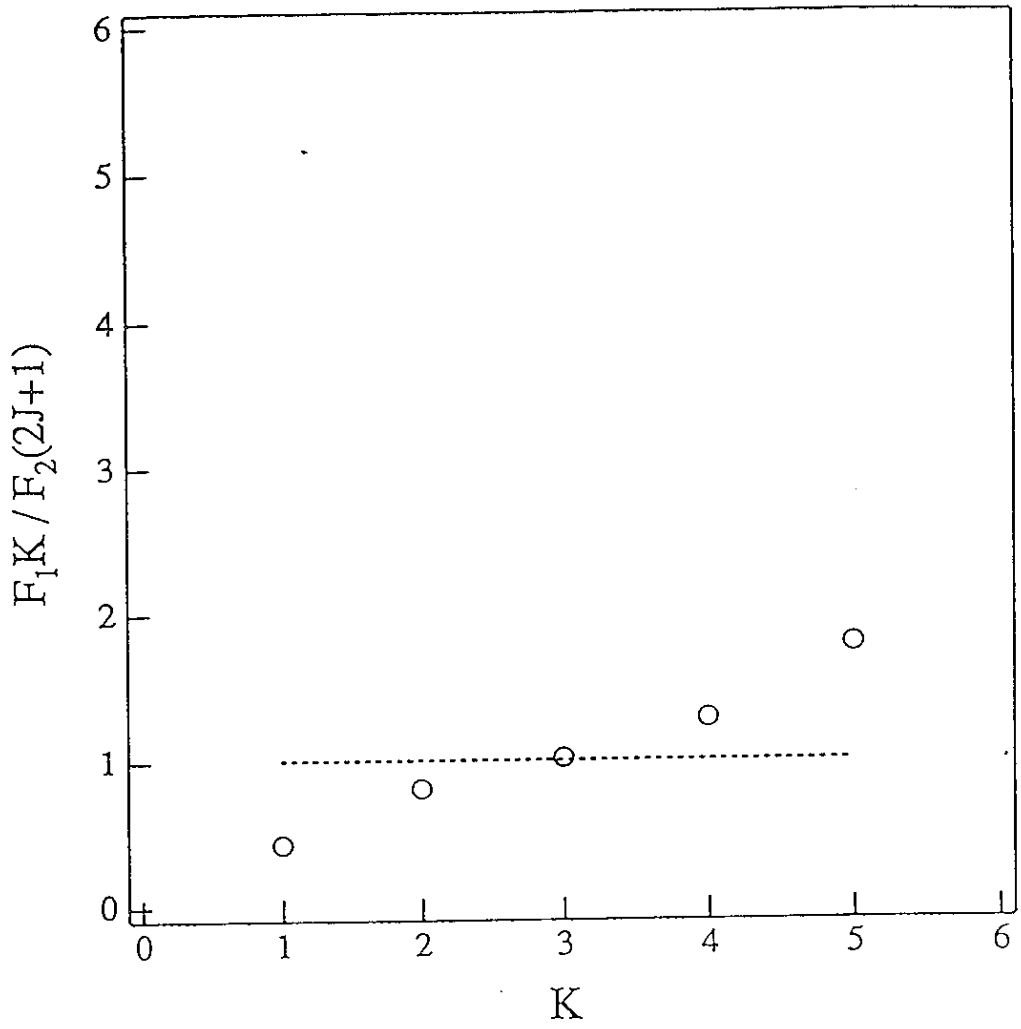

Fig.28. K dependence of spin-orbit population ratios of OH for the reaction $O(^3P)+H_2S$ under the bulk condition.

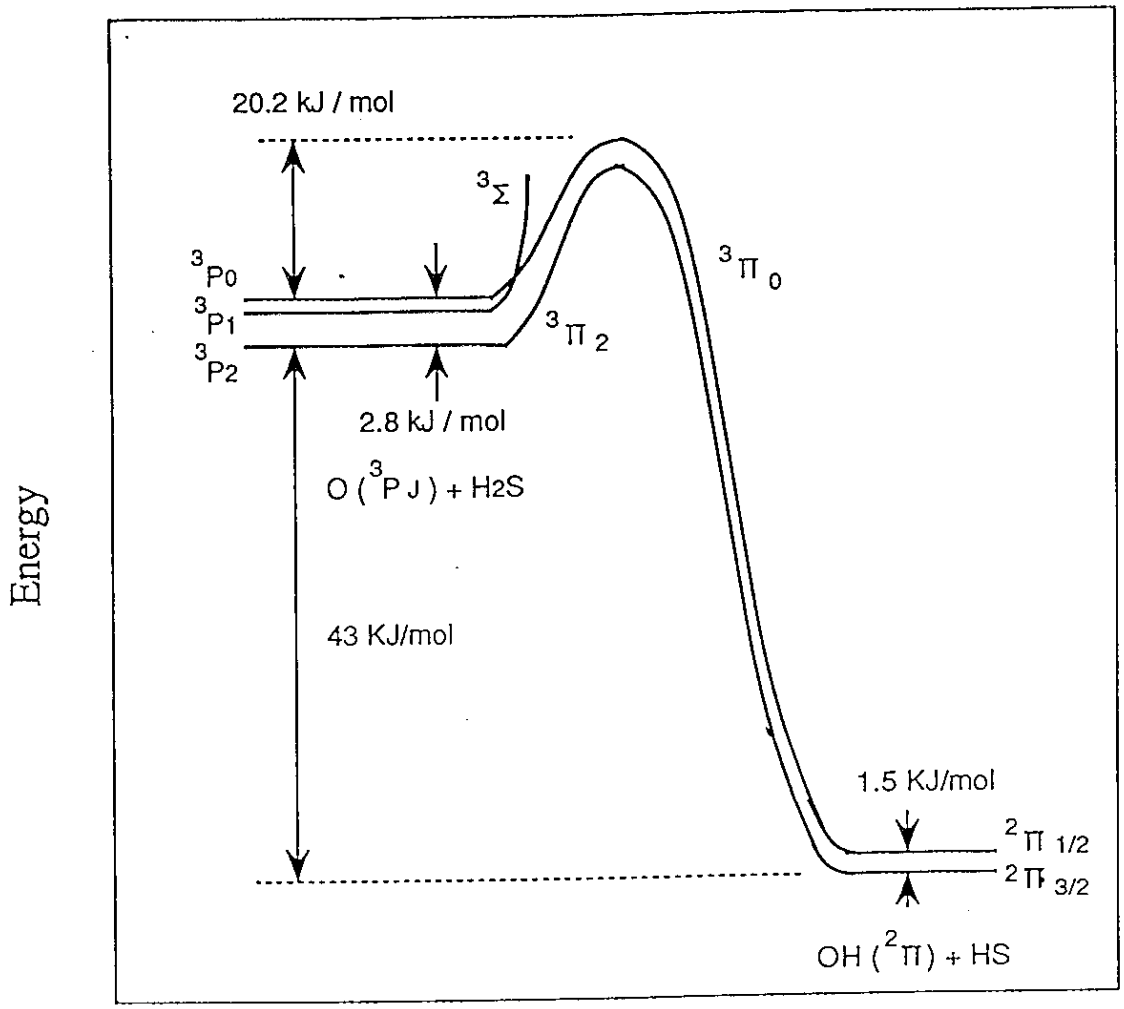

Fig.29. Schematic correlation diagram for the reaction $O(^3P)+H_2S \rightarrow OH+HS$ including the spin-orbit surfaces.

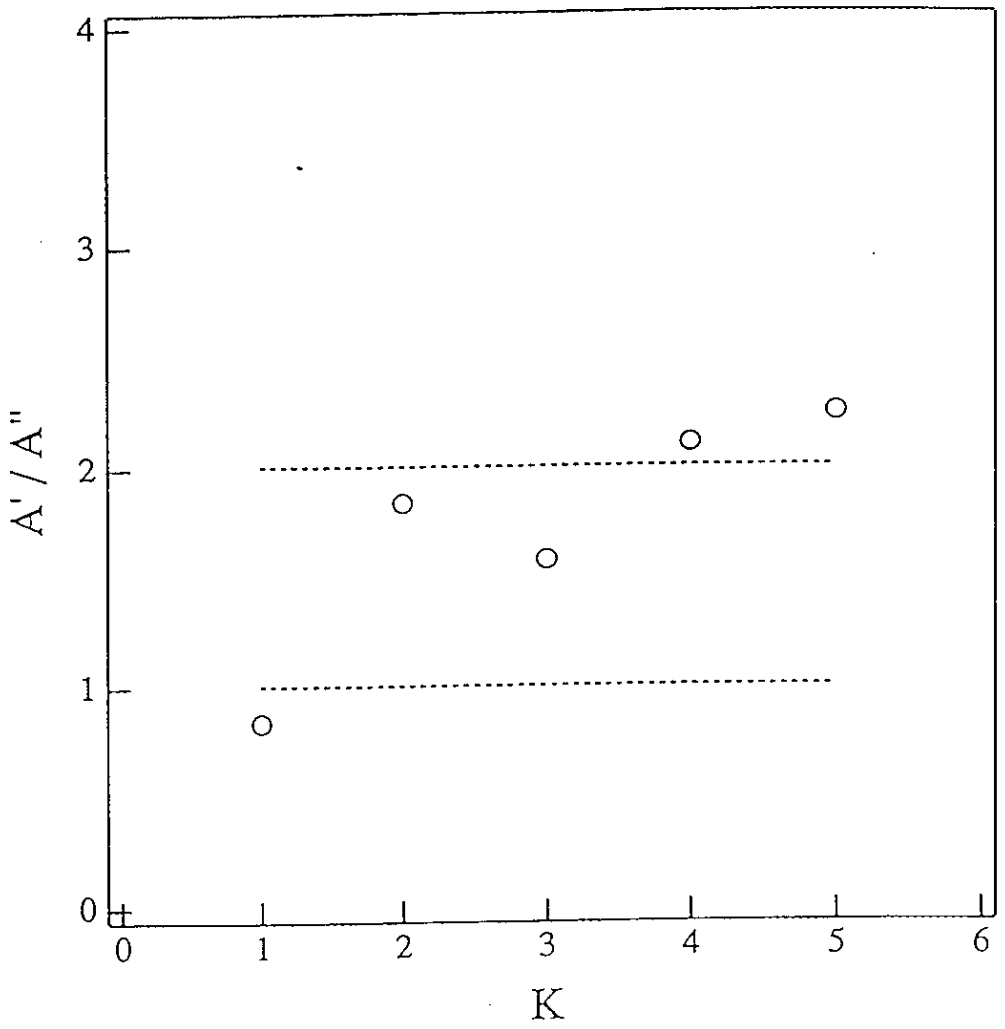

Fig.30. K dependcence of Λ-doublet population ratios of OH for the reaction $O(^3P)+H_2S$ undre the bulk condition.

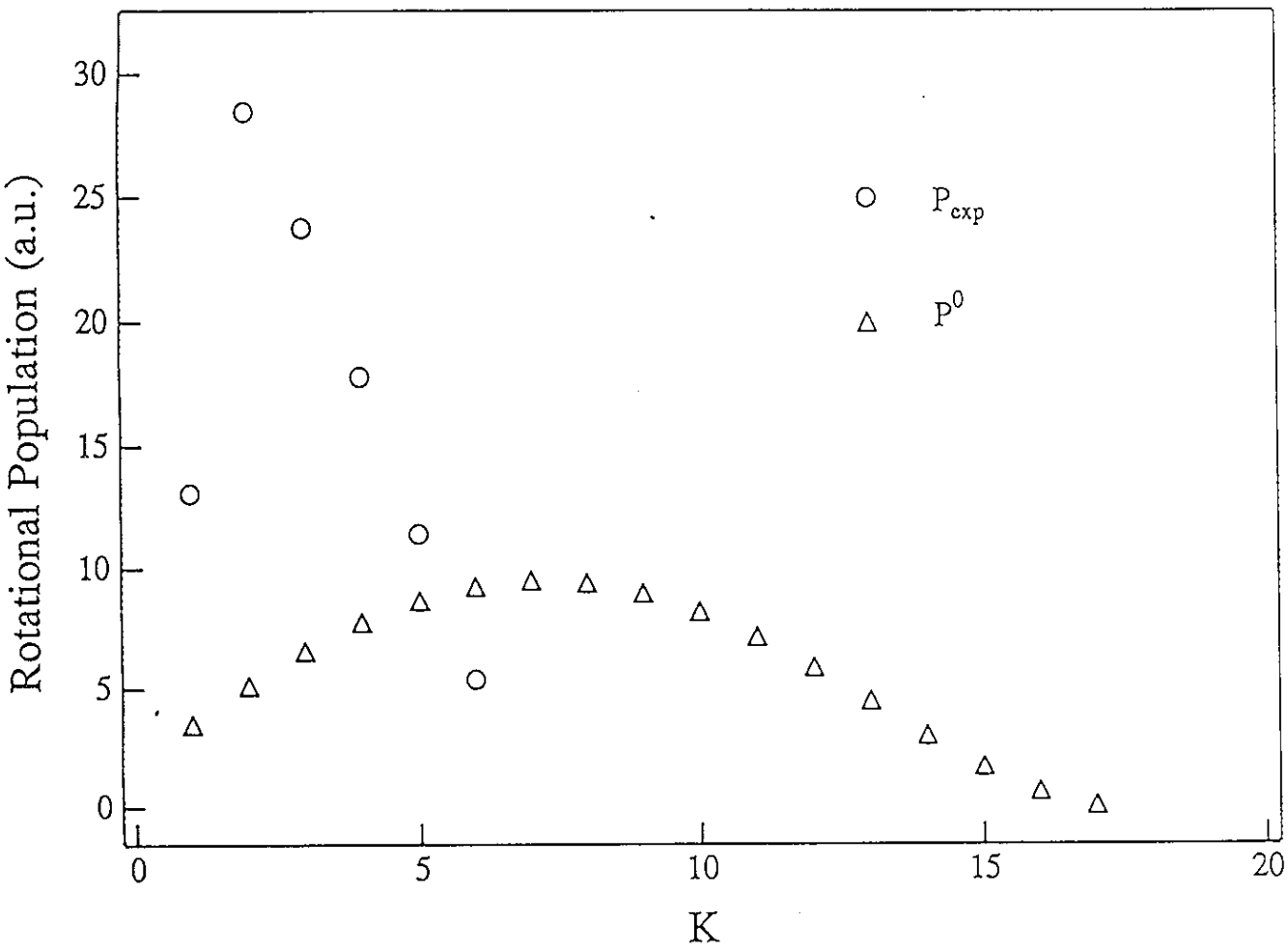

Fig.31(a). Comparisom between experimental and calculated distributions of OH(v"=0) for the reaction $O(^3P)+H_2S$ under the bulk condition.

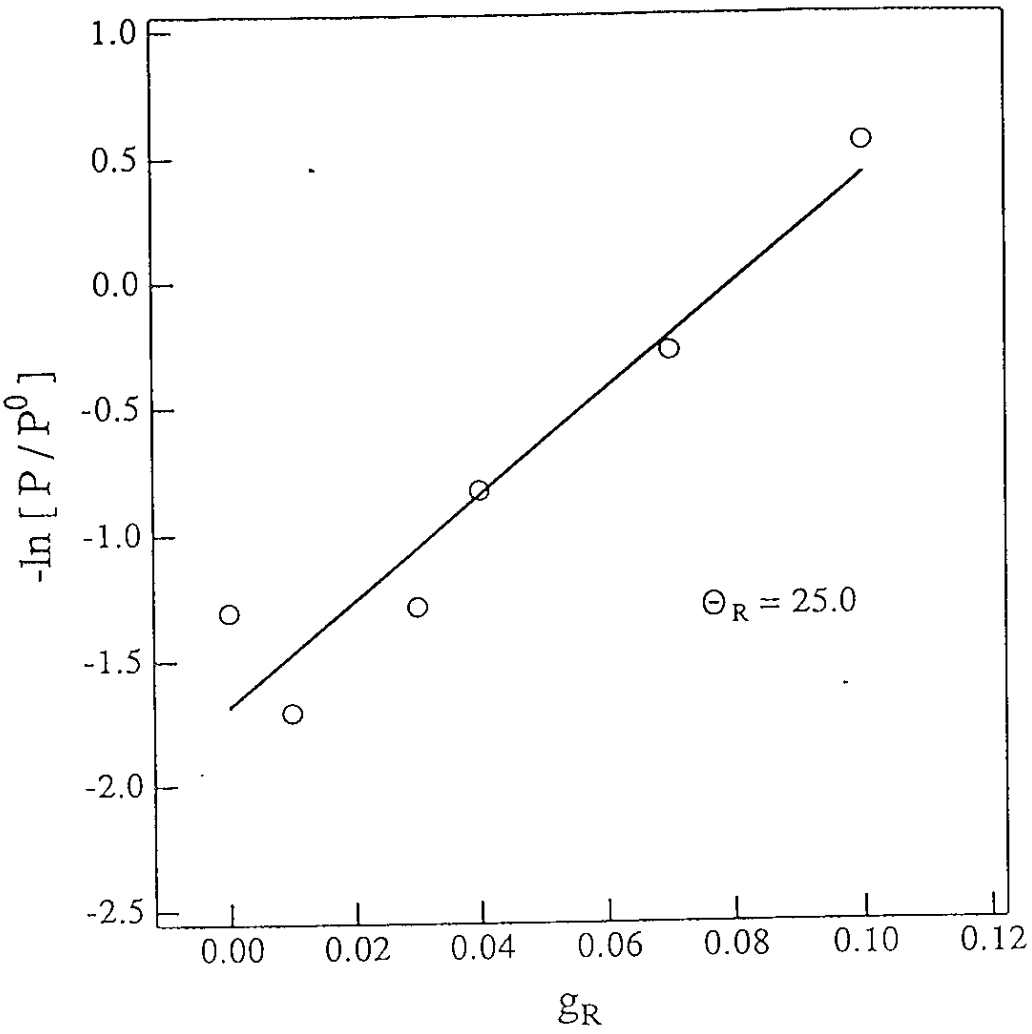

Fig.31(b). Surprisal plot of rotational distribution of OH(v"=0) for the reaction $O(^3P)+H_2S$ under the bulk condition.

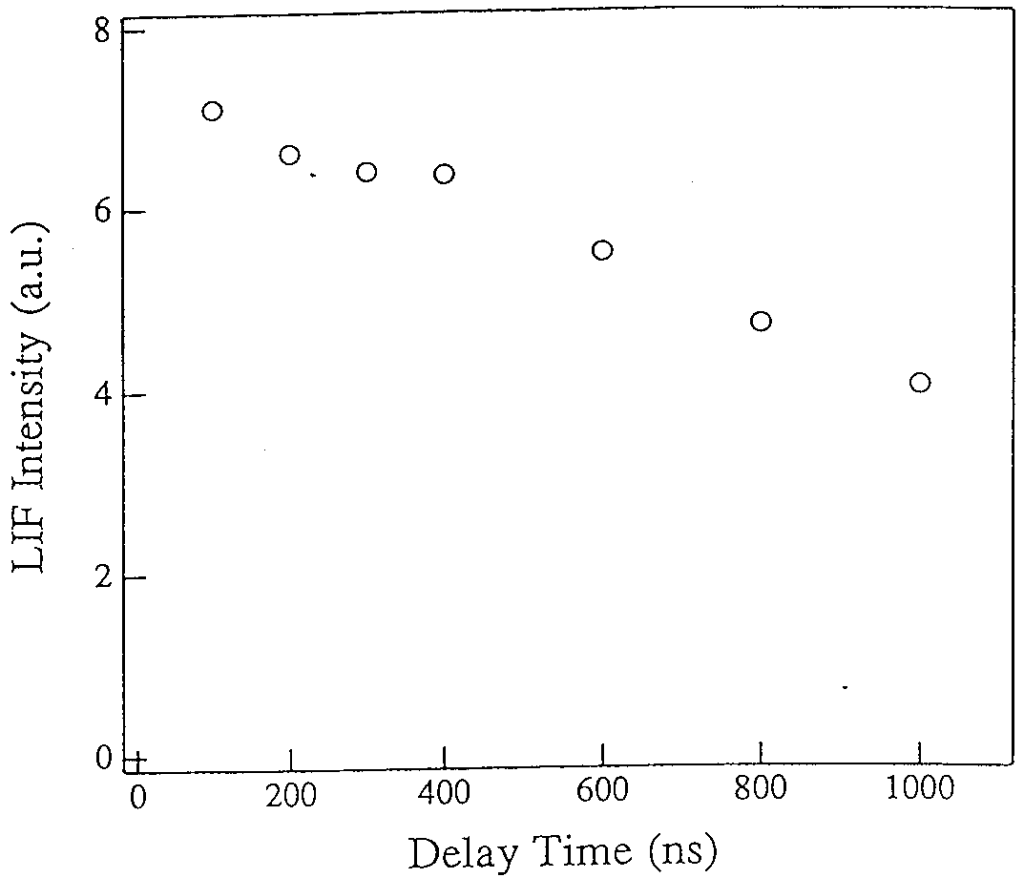

Fig.32. Delay time dependence of the LIF intensity of $OH(X^2\Pi_{3/2}, v''=0)$ for the reaction $HI \cdot N_2O \rightarrow OH+N_2+I$ under the reactant-pair condition.

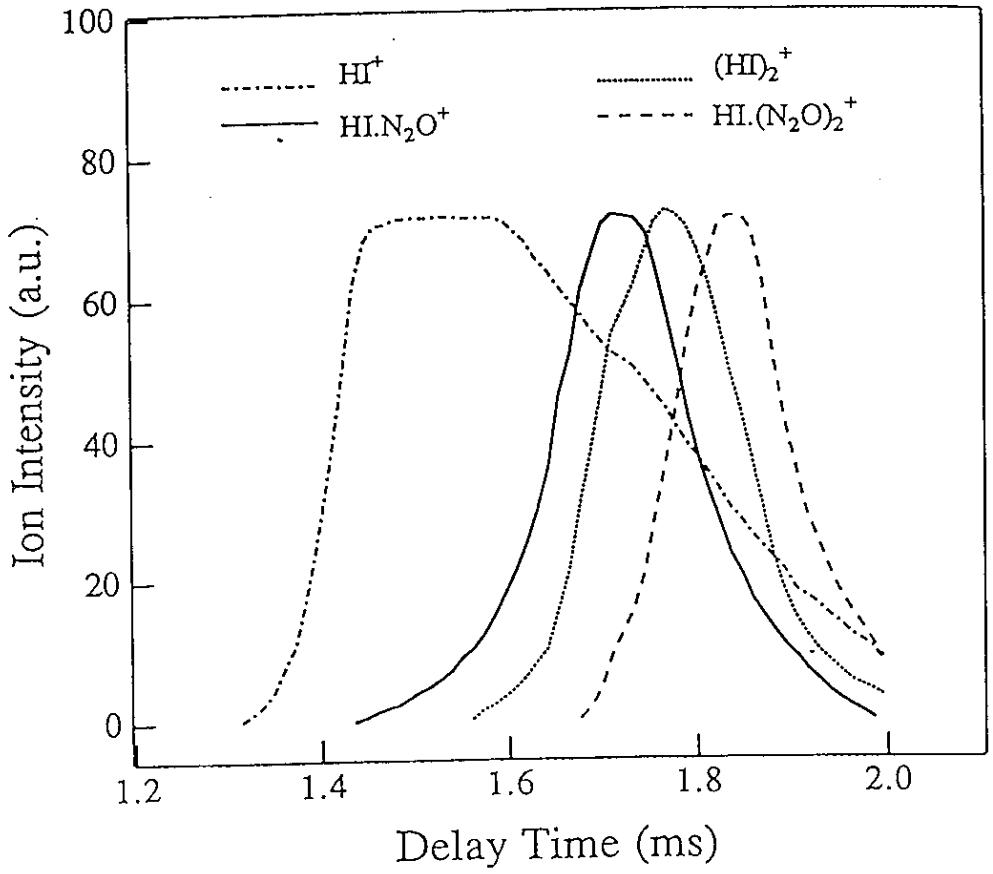

Fig.33. Time profile of $(HI)_N \cdot (N_2O)_M$ clusters generated by the supersonic expansion at the stagnation pressure of 2.0 atm.

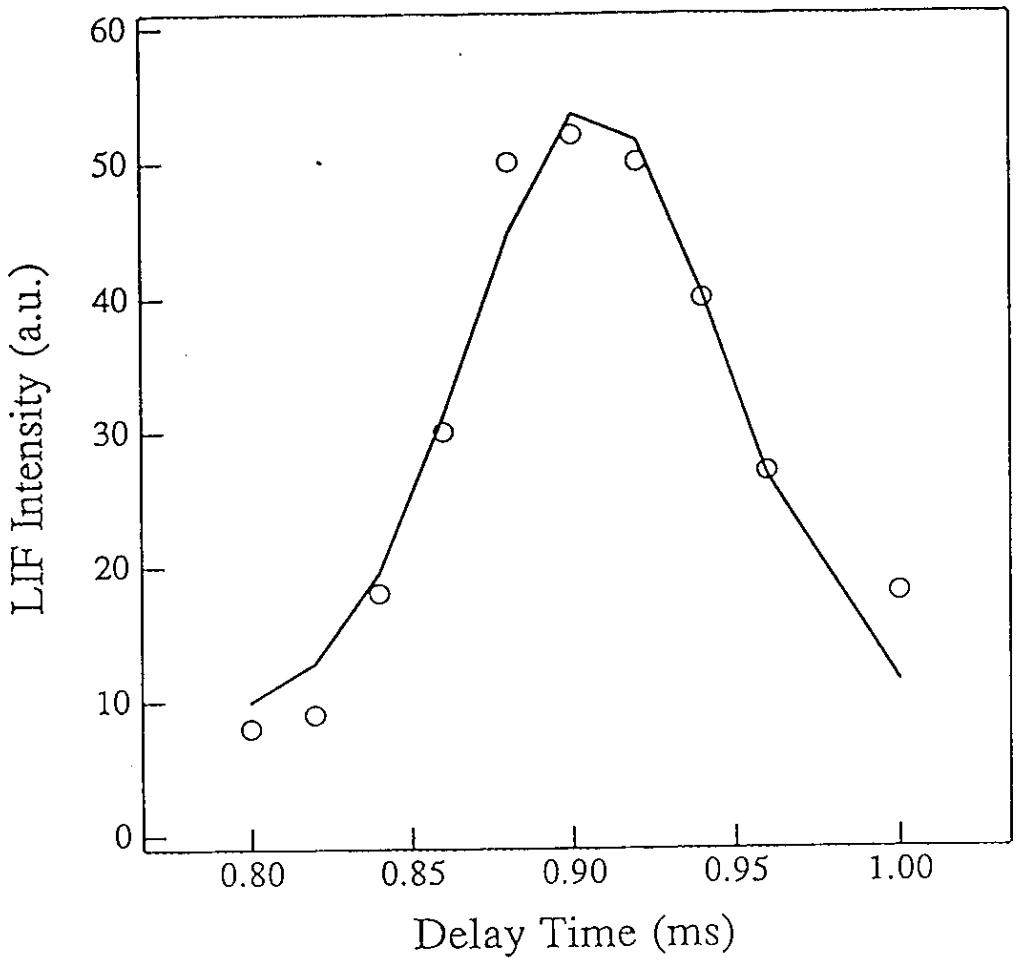

Fig.34. Injector-laser delay time dependence of the LIF intensity of $OH(X^2\Pi_{3/2}, v''=0)$ for the reaction $HI{\cdot}N_2O \rightarrow OH+N_2+I$ under the reactant-pair condition.

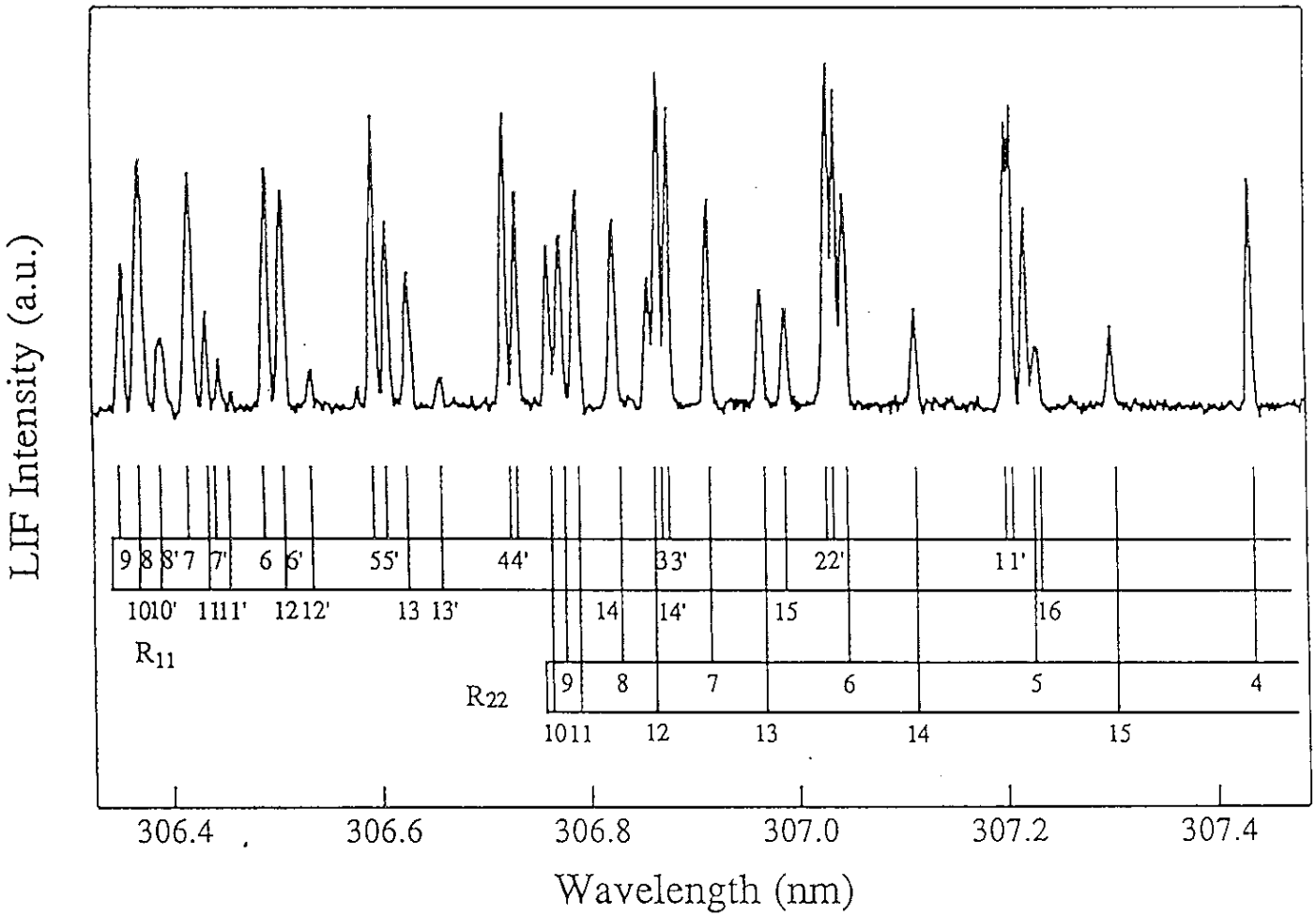

Fig.35. Part of the OH $A^2\Sigma^+$-$X^2\Pi$ v"=0) LIF excitation spectrum for the reaction $HI{\cdot}N_2O \rightarrow OH+N_2+I$ under the reactant-pair condition. (Stagnation pressure is 2.5 atm. Pump-probe delay time is 200 ns. $HI:N_2O:He$ = 2.6:4.4:93.)

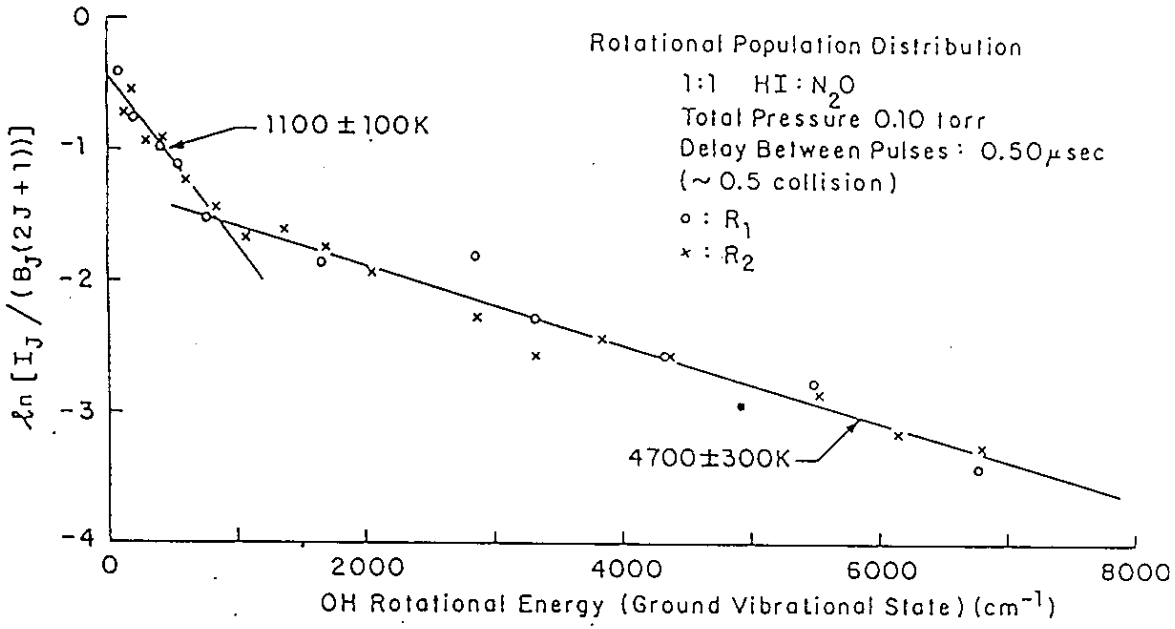

Fig.36. Boltzmann plot of the rotational distribution of OH(v"=0) for the reaction H+N_2O under the bulk condition.

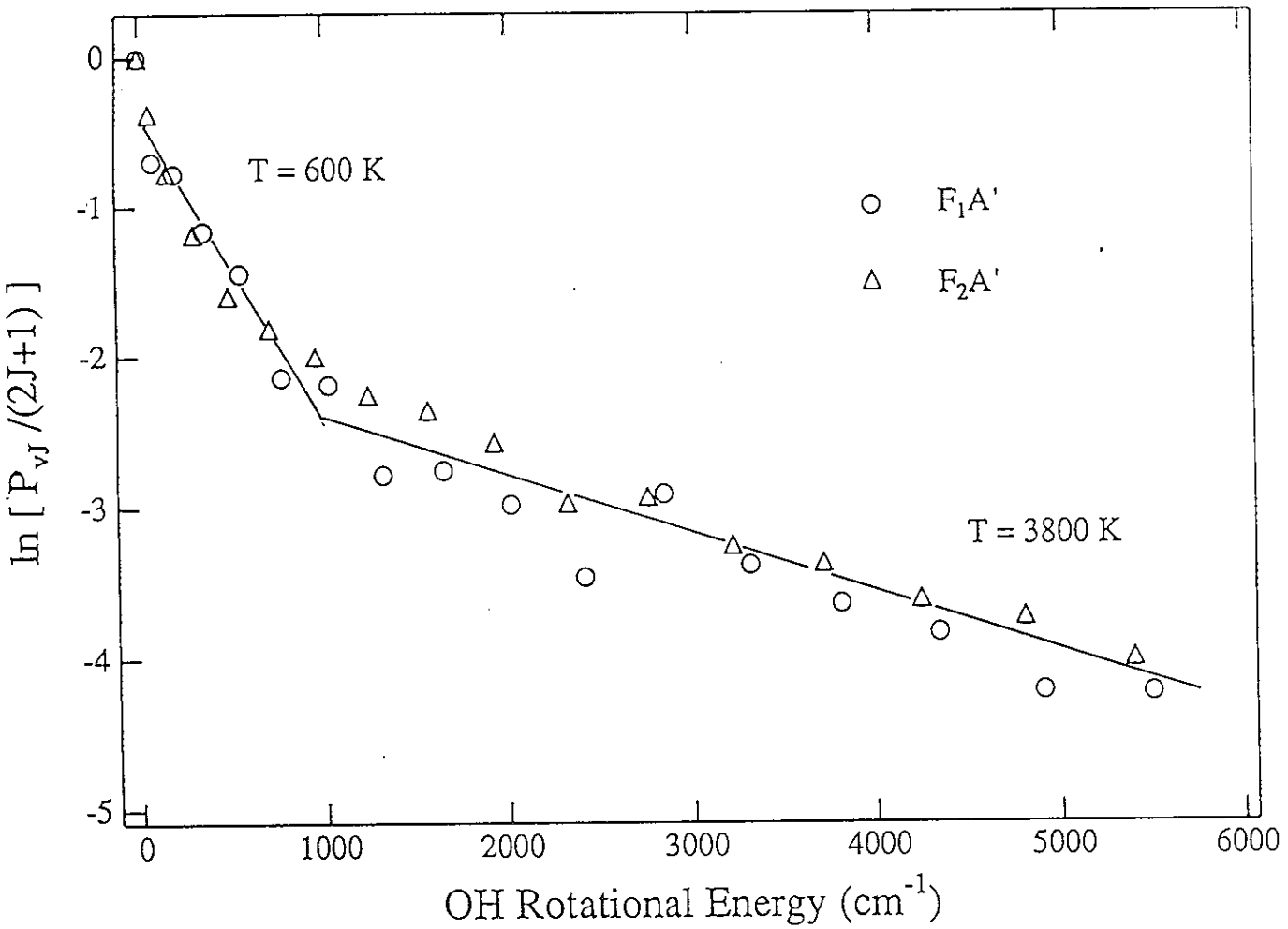

Fig.37. Boltzmann plot of the rotational distribution of OH(v"=0) for the reaction $HI{\cdot}N_2O \rightarrow OH+N_2+I$ under the reactant-pair condition.